Ala. U. RI-8-29317-FTR-Feb 74

cy1

INVESTIGATIONS OF ATMOSPHERIC DYNAMICS USING A CW DOPPLER SOUNDER ARRAY

by

Ganti L. Rao

Final Technical Report

This research work was supported by
the National Aeronautics and Space Administration
George C. Marshall Space Flight Center
Contract NAS8-29317

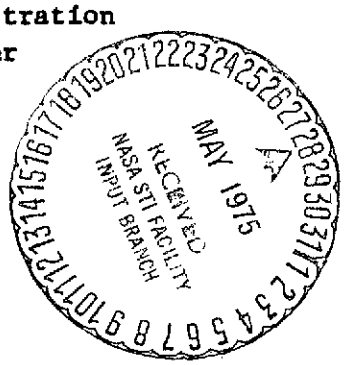

The University of Alabama in Huntsville
Division of Graduate Programs and Research
P. O. Box 1247
Huntsville, Alabama 35807

February 1974

INVESTIGATIONS OF ATMOSPHERIC DYNAMICS USING A CW DOPPLER SOUNDER ARRAY

by

Ganti L. Rao

Final Technical Report

This research work was supported by
the National Aeronautics and Space Administration
George C. Marshall Space Flight Center
Contract NAS8-29317

The University of Alabama in Huntsville
Division of Graduate Programs and Research
P. O. Box 1247
Huntsville, Alabama 35807

February 1974

ACKNOWLEDGEMENT

The author wishes to express his appreciation to Mr. John Jones, National Oceanic and Atmospheric Association, Boulder, Colorado, for building the CW Doppler System; to Mr. B. B. Hensen, Astrionics Laboratory, NASA-MSFC for maintenance of the system; and to Mr. George West, Aero Astrodynamics Laboratory, National Aeronautics and Space Administration, Marshall Space Flight Center for coordination of the entire experimental program.

The author is particularly grateful to Dr. R. E. Smith, Aerospace Environment Division Aero-Astrodynamics Laboratory for his most helpful discussion in conducting this program. This work was performed under contract NAS8-29317 under the technical direction of Dr. R. E. Smith and Mr. George West, Aero-Astrodynamics Laboratory, National Aeronautics and Space Administration, Marshall Space Flight Center, Alabama.

TABLE OF CONTENTS

I. INTRODUCTION

The dynamical state of the ionosphere is distinctive in three respects: tidal oscillations achieve maximum amplitude and exceed the prevailing winds; irregular winds, subject to rapid variation with height, attain an equal intensity; and the turbulent regime of lower levels gives way to a non-turbulent domain above. Extensive observational data of winds and tides at the ionospheric heights using meteor and rocket vapor trail techniques are available in the literature. Analyses of these data reveal strong seasonal variations in the tidal winds, both diurnal and semidiurnal at height near 90 km. Atmospheric oscillations, with periods usually no greater than an hour, are generally called atmospheric gravity waves. These waves (or oscillations) are presumably responsible for perturbations in the neutral and ionized structures of the atmosphere both in the mesosphere and in the lower thermosphere of the terrestrial atmosphere.

Hines (1960) has pointed out that the irregular fluctuations, whose periods are in the 10-30 minute range seen on wind and temperature profiles in the 80-300 km region, are due to atmospheric gravity waves. Perturbations of varying intensities and spatial dimensions are observed in the electron density distribution of the ionosphere. Thitheridge (1963), from the total electron content measurements, showed that the moving perturbations in the ionosphere range from 50-500 km in size. These moving perturbations in the

electron density distribution of the ionosphere are broadly classified as travelling ionospheric disturbances (TID's). The TID's frequently appear in the form of wave-like motions or complexities on the ionosonde records. Several source mechanisms, namely, auroral disturbances, auroral electrojets, severe magnetic storms, and jet streams have been suggested for the generation of TID's. Several local weather disturbances have been suggested as sources for high frequency fluctuations in the F region levels. Recent investigations by Georges (1967), and Baker and Davies (1969), have shown an apparent correlation between tropospheric weather effects and coupling at ionospheric heights. Georges (1967) suggested that observations of a relatively narrow spectrum of waves with periods near 3 minutes were results of the atmospheric filtering of acoustic-gravity waves. Further investigations by Georges (1968), and Davies and Jones (1972), have shown that the following criteria should be satisfied in order to have coupling between the troposphere and the ionosphere :

(1) Cloud tops must be greater than 12 km.

(2) Thunderstorm cells must lie within about 200-250 km from the point on the ground directly below the ionospheric reflection point.

Earlier investigations of ionospheric disturbances have shown an apparent correlation between the neutral atmospheric perturbations and wave-like phenomenon observed on several ground based ionospheric sounding records. The CW (continuous wave) Doppler sounding technique developed by

Davies (1962), and Davies and Baker (1966) was one of the very successful techniques used to monitor ionospheric disturbances on a routine basis. This technique was used in our present investigation of the atmospheric dynamics.

In this report, we present the details of a three-dimensional CW Doppler sounding system currently under operation at the NASA-Marshall Space Flight Center, Alabama, followed by a discussion on the properties of the neutral atmosphere and on the theory of doppler sounding technique. Finally, methods of data analyses used to investigate the dynamical phenomena at the ionospheric heights and suggestions for future investigations are provided at the end of the report.

II. PROPERTIES OF THE NEUTRAL ATMOSPHERE

The primary properties of the atmosphere are its density, pressure, temperature, composition and motion. The density of the terrestrial atmosphere decreases exponentially with increase in altitude. The gravitational field is mainly responsible for making the atmosphere inhomogeneous and also for introducing anisotropy into the propagation of atmospheric waves. A vertically displaced fluid parcel of air experiences a buoyant force which tends to restore the original equilibrium. The rapidity with which the equilibrium is restored characterizes the atmospheric oscillation frequency. A comprehensive theory of atmospheric gravity waves at the ionospheric heights in an isothermal atmosphere was given by Hines (1960, 1968). Recently Wu, et al. (1974) examined the effects of wind shear on acoustic-gravity wave propagation in the thermosphere. When discussing the propagation characteristics of the acoustic-gravity waves in the thermosphere, one can neglect the effects due to the earth's rotation (the Coriolis force), since the wave periods under discussion are less than two hours, and the effects of the electromagnetic field on large scale motions of the atmosphere. The governing equations may be written as (Wu, et al., 1974)

Continuity,

$$\frac{\partial \rho}{\partial t} + \underset{\sim}{\nabla} \cdot (\rho \underset{\sim}{v}) = 0$$

Momentum,

$$\rho \frac{D\underset{\sim}{v}}{Dt} = - \nabla p - \rho \underset{\sim}{g} + \underset{\sim}{\nabla} \cdot \underset{\approx}{\pi}$$

Energy,

$$\rho C_v \frac{DT}{Dt} + p \underset{\sim}{\nabla} \cdot \underset{\sim}{v} = -\underset{\sim}{\nabla} \cdot \underset{\sim}{q} - \underset{\approx}{\pi} : \underset{\sim}{\nabla} \underset{\sim}{v} ,$$

Equation of State,

$$p = \rho RT,$$

where, ρ, v, T, p, $\underset{\sim}{g}$, $\underset{\sim}{q}$, $\underset{\approx}{\pi}$, R, and C_v denote the density, velocity, temperature, pressure, gravitational acceleration, heat flux, stress tensor, universal gas constant and specific heat at constant volume, respectively. The heat flux and the stress tensor can be written as

$$\underset{\sim}{q} = -K \underset{\sim}{\nabla} T$$

and

$$\pi_{\alpha\beta} = -\mu \left(\frac{\partial v_\alpha}{\partial x_\beta} + \frac{\partial v_\beta}{\partial x_\alpha} - \frac{2}{3} \delta_{\alpha\beta} \frac{\partial v_\alpha}{\partial x_\alpha} \right)$$

$$- \zeta \delta_{\alpha\beta} \frac{\partial v_\alpha}{\partial x_\alpha}$$

with K, μ and ζ being the thermal conductivity, and the first and second viscosity coefficients respectively.

Choosing the Z-axis along the vertical height, the x-axis along the eastward direction, and the y-axis along the northward direction, Wu et al.,(1974) obtained the following dispersion relation for acoustic-gravity waves.

$$\tilde{\omega}^4 - [c^2 (k_x^2 + k_z^2) + i \gamma g k_z] \tilde{\omega}^2 +$$

$$[ic^2 k_x k_z - (\gamma-1) g k_x] \frac{d \langle v_x \rangle}{dz} \tilde{\omega} + (\gamma-1) k_x^2 g^2 = 0$$

Introducing

$$K_z = k_z - i \frac{\gamma g}{2c^2} ,$$

we have the following dispersion relation including the effects of wind velocity and wind shear

$$\tilde{\omega}^4 - c^2 (k_x^2 + k_z^2) \tilde{\omega}^2 + [ic^2 k_x k_z - (\frac{3}{2}\gamma - 1) g k_x] \frac{d\langle v_x \rangle}{dz} \tilde{\omega}$$

$$+ (\gamma - 1) k_x^2 g^2 - \frac{\gamma^2 g^2}{4c^2} \tilde{\omega}^2 = 0$$

When the wind velocity and wind shear vanish the above equation becomes identical to the result obtained by Hines (1960).

Hooke (1968) investigated the effects of the passage of internal atmospheric gravity waves on F-region ionization and concluded that the gravity wave induced changes in the values of recombination and loss coefficients in the F-region appear to be small. Following Hooke (1968) in the interpretation of CW doppler array data in terms of internal atmospheric gravity waves, we have assumed that the mechanism for the interaction between atmospheric waves and ionization preserves such wave characteristics as period, phase and group velocities of the wave front. Very large TID's which are, in most cases, accompanied by magnetic storms are interpreted by Georges (1968) as free internal gravity waves with properties determined by the thermospheric parameters. Estimated theoretical wave front tilts (Toltoy, 1963) agree roughly with the observational results of Georges (1968) and Thome (1964, 1968). Observational results on the medium scale TID characteristics appear to fit Friedman's (1966) explanation

in terms of imperfectly ducted internal atmospheric gravity waves in a leaky duct situation and showed that, for a given mode, phase and group velocities are nearly equal and relatively independent of period. The observed medium scale TID speeds of about 300 m sec^{-1} and the apparent direction of TID's travelling away from the winter poles agree with Friedman's (1966) calculations. The observed seasonal variation in the TID propagation direction may be explained by the seasonal variations in the mesospheric temperatures. It is observed that the winter polar mesospheric heatings are frequent and that they affect the mesospheric temperature height profile (Maeda and Young, 1966). The temperature profiles of Champion (1957) do indicate an appreciable weakening of the winter duct around 80 km, compared to the summer, for the middle latitudes. These temperature variations in the mososphere cause leaky duct conditions which allow atmospheric gravity wave energy to penetrate to F-region levels to support the wave propagation.

III. RADIO SOUNDING OF THE IONOSPHERE

A model C-4 type conventional swept frequency ionosonde, a pulsed phase path sounder, a three dimensional CW doppler sounder array, and an airglow observatory are currently in operation. A summary description of the phase path sounding system and measurements follows:

The electric field intensity $E(\xi)$ of a radiowave at some point ξ on the ray can be expressed as

$$E(\xi) = A(\xi)\, E_{xp}\ [\, j\ (\omega t - k_o \int_0^{\xi} \mu\, ds)\ ]$$

where the integral is taken along the ray from some arbitrarily chosen origin $\xi = 0$. Then, at any instant t, the difference in phase $\Delta\phi$ between the signal at the point ξ and the signal at the origin is given by

$$\Delta\phi = k_o \int_0^{\xi} \mu\, ds = \frac{2\pi}{\lambda o} \int_0^{\xi} \mu\, ds\ .$$

Since $\Delta\phi/2\pi$ is the number of vacuum wavelengths represented by the difference in phase, we see that the integral

$$p = \int_0^{\xi} \mu\, ds$$

yields a distance equal to the total length of the specified number of vacuum wavelengths. This quantity p is called the phase path of a radio wave passing through the ionosphere.

Two different techniques are presently employed for making phase path measurements. The first method consists of transmitting fixed

frequency pulses with coherent detection used to indicate the phase of the echo relative to a stable reference. This technique also provides accurate determination of the group paths. Measurements of phase paths and group paths of radio waves as a function of frequency are presently being made using this phase path sounder system. The pertinent specifications of the phase path sounder system are listed in Table 1.

The second method of measuring phase is by using a continuous wave doppler sounding technique. When a radio wave of a constant frequency f is transmitted from a stable transmitter and received via ionospheric reflection, it is observed that the frequency of the received signal fluctuates slightly. The frequency fluctuations for ionospheric propagation are usually of the order of a few Hertzs. These perturbations are related to changes in the phase path of the probing signal. The relation connecting frequency fluctuations and phase path variations in the absence of earth's magnetic field can be expressed as (Davies, 1965)

$$\Delta f = \frac{-f}{c} \frac{dp}{dt}$$

where

f = transmitted frequency, c = speed of light in free space,

p = μds = phase path

and μ is the refractive index along the ray path s. The phase path, and hence Δf, are functions of both μ and s. Several relations connecting the doppler frequency variations and ionospheric parameters are summarized in Table 2. Contributions to the frequency variations may occur along the radio path

within the ionosphere, but due to the $1/\mu$ factor, the region near reflection seems to be the most effective for producing the perturbations in the probing frequency. A frequency shift can result from either of the two following effects, or a combination of both.

(1) change in ray path (s) caused by change in the height of reflection, or

(2) change in refractive index (μ) along the path caused by change in electron density below the level of reflection.

Considering the first case, if we assume mirror-like reflection at a height h, with no changes in refractive index below h, then

$$\frac{dp}{dt} = -2 \frac{dh}{dt}$$

$$\Delta f = \frac{2f}{c} \frac{dh}{dt}$$

for a given rate of change of reflection height

$$\Delta f \propto f$$

In the second case, if we assume a constant height of reflection and change in electron density below the level of reflection then,

$$\Delta f \propto 1/f$$

In reality the situation is more complicated, but the important point is that the variation of Δf with f gives an indication of the cause of the doppler shift Δf. An important case where doppler shifts are not dominated by reflection heights is that of solar flare ionization enhancements due

the radiowave and the atmospheric disturbance is not known. This can be resolved from ionosonde measurements.

Davies, et al., (1969) showed the analogies between some magneto-ionic ray formulas and corresponding formulas for neutral atmospheric waves in an isothermal atmosphere. The acoustic waves are analogous to radio waves of frequencies greater than the electron gyrofrequency (f_H), whereas atmospheric gravity waves are somewhat similar to whistler waves. Some of the comparisons between atmospheric waves and radio waves are presented in Tables 3 and 4.

IV. DATA OVERVIEW AND METHODS OF ANALYSIS

The visible record of the doppler data is obtained by frequency analysis of the signal. The frequency analysis is carried out by using a UA6B Ubiquitous audio spectrum analyzer. The output from the spectrum analyzer is displaced on a facsimile chart. About two weeks of data tape may be played back producing about 20 feet of facsimile chart record. It is not proposed to analyze the complete data thatare being collected, but instead to study specific atmospheric-ionospheric events seen clearly on the doppler record. The initial 20 feet of facsimile chart record containing approximately two weeks of data are being used to identify specific events such as travelling ionospheric disturbances, and thunderstorm, solar flare and magnetic storm effects. After visual identification of the events, the segments of the data tape containing the events are played back at a slower speed for better time resolution. By playing back the tapes at a slower speed and recording the data, one can achieve a time resolution of about five seconds to study the fine structure in the doppler variation. The specific identified segments of the analog doppler data are recorded on a separate tape and sent to the computer laboratory of NASA-MSFC. These data are then digitized at ten second intervals for further analysis.

The geographic location of the array is shown in Table 5. The spaced transmitters are located at Muscle Shoals, Alabama, at Nickajack Dam, Tennessee, and at Fort McClellan, Alabama. As mentioned earlier, one of the aims of the

program is to determine the horizontal and vertical trace velocities of the TID's and then determine the speed, elevation and azimuth of a travelling ionospheric disturbance from the recordings of all nine field transmitters. The following methods are used to derive the characteristics of the travelling ionospheric disturbances.

The horizontal and vertical phase velocities are determined from the doppler records by determining the relative time displacements. Imagine that a plane wave front is moving across the array system as shown in Figure 1. Let τ_{MN} and τ_{MF} be the time delays between the reflection points M-N and M-F respectively. Here M, N, and F refer to the ionospheric reflection points corresponding to the transmitters located at Muscle Shoals, Alabama, Nickajack Dam, Tennessee, and Fort McClellan, Alabama, respectively. The apparent trace velocities V_{MN} and V_{MF} are given by the following relations:

$$V_{MN} = \frac{MN}{\tau_{MN}} \quad \text{and} \quad V_{MF} = \frac{MF}{\tau_{MF}}$$

The magnitude of V_H and the direction ϕ (measured east from north) can be determined from the following set of equations

$$\text{Cot } \phi = -\frac{V_{MN} \text{ Sin } \psi_{MN} - V_{MF} \text{ Sin } \psi_{MF}}{V_{MN} \text{ Cos } \psi_{MN} - V_{MF} \text{ Cos } \psi_{MF}}$$

and the magnitude of V_H is given by

$$V_H^2 = \frac{V_{MN}^2 \, V_{MF}^2 \, \text{Sin}^2 \, (\psi_{MF} - \psi_{MN})}{V_{MN}^2 + V_{MF}^2 \; 2 \, V_{MN} \, V_{MF} \, \text{Cos} \, (\psi_{MF} - \psi_{MN})}$$

where ψ_{MN} and ψ_{MF} are the angles between the geographic north and the lines MN and MF respectively. The true velocity may be determined by computing the vertical trace velocity V_V. The vertical trace velocity V_V may be determined from the time displacements at various frequencies and the difference of reflection points for a given transmitter and receiver location, are assumed to lie on a vertical plane. The heights of reflections for various frequencies involved are determined from the ionogram analysis. From the values of horizontal phase velocity V_H and vertical trace velocity V_V, the true phase velocity may be determined as shown in Figure 2.

For a given sample of the doppler sounder record, the time displacements are determined by computing the cross-correlation functions. Consider two time series functions given by f(t) and g(t). The cross-correlation coefficients of f(t) and g(t) are given by

$$C_{fg}(\tau) = \frac{1}{S_f S_g} \left\{ \frac{1}{t_1 - t_o} \int_{t_o}^{t_1} [f(t) - \bar{f}]\,[g(t+\tau) - \bar{g}]\, dt \right\}$$

where

$\bar{f}$ and $\bar{g}$ are the time averages of f(t) and g(t).

τ is the time displacement between the two functions being correlated.

S_f and S_g are the standard deviations of f(t) and g(t) where

$$S_f = \left[\frac{1}{t_1 - t_o} \int_{t_o}^{t_1} [f(t) - \bar{f}]^2\, dt \right]^{1/2}$$

$$S_g = \left[\frac{1}{t_1 - t_o} \int_{t_o}^{t_1} [g(t) - \bar{g}]\, dt \right]^{1/2}$$

The auto-correlation coefficient is given by

$$R_{ff}(\tau) = \frac{1}{(S_f)^2} \left\{ \frac{1}{t_1 - t_o} \int_{t_o}^{t_1} [f(t) - \bar{f}]\, [f(t+\tau) - f]\, dt \right\}$$

The time interval t_1 is the period the ionospheric disturbance lasted on the doppler sounder record.

The characteristics of some of the wavelike ionospheric disturbances seen on CW doppler sounder records are subjected to power spectral analysis to investigate the wave characteristics. One of the characteristics of the ionosphere is the electron density variability with time at a given place. The ionosphere may be treated as a quasi-stationary random phenomenon since several unknown processes are in operation in any given situation. Power spectral analysis is often used to investigate the characteristics of the quasi-stationary random process. Tolstoy and Montes (1971) successfully used power spectral analysis of CW doppler sounder data to investigate the phase height fluctuations in the ionosphere between 130 and 150 km. The general problem of spectrum analysis was formulated by Blackman and Tukey (1959).

Consider a cross-correlation function of two time series

$$\rho_{12}(\tau) = \underset{T \to \infty}{Lt}\ \frac{1}{T} \int_{-T/2}^{+T/2} f_1(t) \cdot f_2(t+\tau)\, dt$$

where $f_1(t)$ and $f_2(t)$ are two time series, T is the length of the CW doppler record, and τ is the time lag of f_1 relative to f_2. In special case when $f_1 = f_2$ equation (1) becomes the auto correlation function

$$\rho_{11}(\tau) = \frac{Lt}{T \to \infty} \frac{1}{T} \int_{-T_2}^{T_2} f_1(t)\, f_1(t+\tau)\, dt$$

The power and cross power density spectrums are obtained by Fourier transforming the auto and cross correlation functions respectively, as follows:

$$\rho_{11}(\omega) = \frac{1}{2\pi} \int_{-\infty}^{+\infty} \rho_{11}(\tau)\ e^{i\omega\tau}\ dt$$

$$P_{12}(\omega) = \frac{1}{2\pi} \int_{-\infty}^{+\infty} \rho_{12}(\tau)\ e^{-i\omega\tau}\ dt$$

where ω is the angular frequency in radians per unit time. In general the cross correlation function is asymmetrical and therefore the cross spectrum function would be complex

$$P_{12}(\omega) = C_o(\omega) + i\, Q_{uad}(\omega)$$

where $C_o(\omega)$ is the real part and $Q_{uad}(\omega)$ is the imaginary part of the cross spectrum function.

The phase relationship between frequencies is given by

$$\Delta\,\theta\,(\omega) = \theta_2(\omega) - \theta_1\,(\omega) = \tan^{-1}\left[\frac{Q_{uad}\,(\omega)}{C_o\,(\omega)}\right]$$

where $\theta_1(\omega)$ phase of time series $f_1(t)$

$\theta_2(\omega)$ phase of time series $f_2(t)$

The coherence estimates are given by

$$|\gamma\,(i\omega)|^2 = \frac{|P_{12}\,(\omega)|^2}{P_{11}(\omega) \cdot P_{22}(\omega)}$$

where $|\gamma(i\omega)|$ is the magnitude of the complex coherence.

The amplitude of the cross spectrum at each frequency is the product of the corresponding amplitudes in the two time series. If a particular spectral component is absent from either series, then it will be absent in the cross-spectrum and the coherence will be a minimum at that frequency.

Blackman and Tukey (1959) have recommended that in order to minimize leakage from the low frequencies to the high frequencies, the data should be pre-whitened prior to the power spectrum analysis. This may be accomplished by applying to the data a simple derivative filter. The smoothed spectral estimates may be obtained by using a 'hanning window' which has side lobes of the order of 1% of the main lobe. The number of lags are usually equal to 10% of the data sample giving 20 degrees of freedom.

The lowest frequency that can be analyzed in the data sample is determined by the maximum lag, τ_m since $f_{min} = (2T)^{-1}$. The digitization interval, Δt, determines the highest frequency, $f_{max} = (2\Delta t)^{-1}$. The pre-whitening filter may be restored by multiplying each frequency estimate by the inverse of the square of the amplitude response at that frequency.

V. ATMOSPHERIC-IONOSPHERIC DISTURBANCES

A summary of the observations using NASA-MSFC Doppler Sounder array is presented and discussed here. The experimental results obtained from New York Doppler Sounder array are also analyzed and the results are presented here. The technical details and geographic location of the New York Doppler Sounder array are given in a report by Rao (1972).

A typical doppler sounder recorder from the NASA/MSFC array, showing the doppler variations (phase path variations) over a 24 hour period for the operating frequency 4.0125 MHz is shown in Figure 3. It can be seen from the figure that during the day time the doppler variations are quite narrow with small and rapid frequency fluctuations. Sunrise effects on the doppler record are shown around 0530-0600 CST. During sunrise conditions, there is an increase in the electron density of the ionosphere due to photo-ionization. The increase in the electron density causes a decrease in the radio phase path length, which appears as an increase in doppler shift in frequency. After the sunrise effects, the doppler variations remained fairly constant with localized small rapid frequency fluctuations superposed on the record. These rapid frequency fluctuations are mainly due to the changes in the electron density near the reflection levels caused by the rapid production and loss mechanism of electrons due to the solar radiation and the movement of localized small scale ionospheric irregularities. The doppler sounding technique of the ionosphere is capable of separating the magneto-ionic components of the electromagnetic wave propagating in the

ionosphere when there is a large doppler shift in the observations. The separation of the magneto-ionic components is seen from Figure 3 in which a weak trace is shown on the main doppler trace during the periods between 1800-0400 CST indicating the presence of an extraordinary magneto-ionic mode. It can also be seen from the figure that the doppler variation between 1800 and 0200 CST shows large fluctuations indicating the presence of wave-like phenomena. Such events seen on the doppler records are classified as travelling ionospheric disturbances (TID's). Examination of several days of doppler records taken at fixed frequency transmission under quiet ionospheric conditions indicate a general trend that the variations are small during day time hours whereas the night time variations are large. This variability in the doppler fluctuations may be due to the reflection height changes from the daytime to the night time on fixed frequency sounding records and the predominant occurrence of TIDs during sunset and night time conditions. On the high-frequency soundings (especially when operated near the F2 layer critical frequency) the doppler signal is either lost or a diffuse trace is recorded. Under spread F conditions, the doppler record becomes very diffuse and a wave like pattern is noticed in the diffused (often lost) trace of the doppler record. These investigations are currently under progress from the data that are being collected using the NASA/MSFC doppler sounder array.

Travelling Ionospheric Disturbances

Some of the typical TIDs observed on our doppler sounder array are shown in Figures 4, 5, 6, 7 and 8. Usually the TIDs are observed as a wave like fluctuation on the doppler sounder record. The disturbance first appears on

the high frequency sounding records followed by middle low frequency sounding records. It is also observed from the typical TID's recorded on the doppler system that the amplitude of the doppler fluctuations are larger for higher sounding frequencies and lower for the lower sounding frequencies. The TID's are generally interpreted as manifestations of internal atmospheric gravity waves (Hines, 1960). The characteristics of the internal gravity waves are that the amplitude of the waves increases with altitude. This is observed on the doppler records as the perturbation amplitude increased with the probing frequency. The CW doppler data for several TID events for the NASA/MSFC array are under analysis and the results will be reported later.

During the period of this investigation, we have analyzed some of the TID data collected from a CW doppler sounder array located in the New York area (41°N, 74°W) and the results are reported here. The horizontal phase velocities for the TID events observed during winter (November, December 1969 and January 1970) and equinoctial (October 1969, February, April 1970) conditions have been computed. The diurnal variation of phase speeds for winter and equinoctial seasons are shown in Figures 9 and 10, respectively. The daytime winter speeds range from 70 to 140 m sec^{-1} whereas the night time winter values are higher and in the range of 140-340 m sec^{-1}. There are not many day time equinoctial TID events available; but, in general, the day time speeds are lower than the night time. Also

comparison of figures indicatesthat TID activity is more predominant in the winter than at the equinoxes. TID's were observed on the CW doppler records from sunrise to late midnight during the winter whereas during the equinoctial months, the major TID activity occurred during the sunset and post sunset periods. The diurnal variation of TID propagation (directions heading) during the winter and equinox seasons are shown in Figures 11 and 12 respectively. In winter TID's propagate to the Southeast during daytime and towards the Southwest during the nighttime. It appears, in general, that the TID's propagate generally in the north-south direction during winter seasons. The predominant propagation direction is between west and southwest during equinoctial conditions.

TID observations in the northern and southern hemispheres, as reported by various investigators, are summarized in Table 6. Munro (1950, 1953), from an extensive study of medium scale TID's for southern hemisphere locations, reported that the mean directions of travel were northward in winter and eastward in the equinoctial months. The horizontal speeds varied from 85 - 170 m sec^{-1}. From the results of the present investigation, as well as those of earlier investigations, it appears that during winter and summer periods TID's travel away from the winter poles. During equinoctial seasons, the TID's in the northern hemisphere have an apparent westwood motion while those in the southern hemisphere have an eastward motion. Examinations of Table 6 also show that large scale disturbances are either accompanied by a magnetic storm or associated with some form of auroral zone activity. On

the other hand, medium scale TID's are not generally correlated with the auroral or magnetic activity.

Severe magnetic storms and auroral electrojets were shown to be sources for large scale TIDs, (Hunsucker and Treten, 1967; Flock and Hunsucker, 1968; Thome, 1968). The results of the present investigation and the summary results from Table 6 indicate that the sources for the majority of the TID events are located in polar region. Some type of auroral activity occurs almost every night. Magnetic storms as well as particle precipitation cause intense auroral activity. The most important mechanisms for generating atmospheric gravity waves operate in the auroral zone; neamely, joule heating due to auroral electrojets, heating due to particle precipitation and the motions imparted to the neutrals by the motions of the charged particles. These source mechanisms may be responsible for generating large scale TID's which can propagate long distances. Even if there are no magnetic storms to generate currents and other disturbances, still the night time auroral zone is active with visual aurora forms moving with supersonic speeds, which appear to be responsible for auroral infrasonic waves (Wilson 1967). Particle precipitation is a regular phenomena which in turn causes heating and movement of neutrals by the charged particle motions. Several cumulative effects operating in the auroral zone during disturbed and quiet conditions could be responsible for generating waves. Active auroral conditions during the night apparently cause higher speeds and longer wavelengths for night time TID events.

VI. CONCLUSIONS

The following are some of the conclusions drawn from the study.

1. During summer and winter seasons in both hemispheres, the TID's travel away from the winter polar regions. During equinoctial months, disturbances in the northern hemisphere travel approximately westward while those in the southern hemisphere travel eastward.

2. The daytime speeds are lower and periods are usually shorter than night time values. The daytime values are in the range of 70 - 140 m sec^{-1} and the night time values are in the range of 140 - 340 m sec^{-1}. The TID activity appears to be predominant during the winter season.

3. The large scale TID's are usually either accompanied by a magnetic storm or associated with some form of auroral zone activity. The medium scale TID's are not generally correlated with either auroral or magnetic activity.

4. The observed seasonal variation in TID propagation direction may be explained by mesospheric temperature variations. Observational data (Champion 1957) indicate that there is an appreciable weakening of the winter duct around 80 km due to mesospheric warnings. These temperature variations in the mesosphere cause leaky duct conditions which allow the gravity wave energy to penetrate to F-region levels.

5. Auroral zone activity appears to be the reason for the longer periods and higher speeds of the night time TID's.

VII. SUGGESTIONS AND PROPOSED STUDIES

Evidence for relationships between meteorological and ionospheric phenomena has been advanced by several investigators (for example, Baker and Davies, 1968; Georges, 1968). A CW doppler sounder array was in operation at Huntsville, Alabama, during 1967-68 to investigate the coupling between the troposphere and the ionosphere at times of static test firings of Saturn rocket engines to see whether the acoustic energy released at the ground level reached ionospheric levels. The static test firings of Saturn rocket engines did not provide any conclusive evidence of acoustic energy leaking from the ground to the ionospheric levels (W. T. Roberts, Personal Communication). However, the CW doppler data (provided by W. T. Roberts) did indicate an evidence of coupling between tropospheric source and the ionosphere at the times of severe local thunderstorm activity. About 80% of high frequency CW doppler fluctuations with periods less than or equal to six minutes, were well correlated with the local thunderstorm activity. Figure 13 is a typical event showing the thunderstorm correlated doppler fluctuations.

The present three dimensional array of the NASA/MSFC is more sophisticated and better designed to study the coupling between tropospheric sources, ie. thunderstorm effects and the ionosphere. The North Alabama region is generally very active for severe thunderstorms and tornadoes and our array is ideally located to study the statistical nature of this apparent correlation.

The atmospheric layers between 90-200 km (where the temperature begins to climb and the molecular weight changes)is rather poorly understood. These changes produce a zone where acoustic cut-off frequency (W_a) can become less than Brunt-Vaisala frequency (W_b). This is so called anomalous zone where $W_b > W_a$ (Johnston 1967). The dispersion diagrams (Tolstoy 1963) show that there exists a region where one cannot distinguish between acoustic and gravity waves. The dispersion characteristics of the naturally occurring wave trains (TIDs) whose propagation characteristics are controlled by the atmospheric structure between 90-200 km may be used to investigate thermospheric wave propagation.

The phase height fluctuations in the ionosphere may be investigated using the CW doppler data and power spectral analysis. The variation of spectral peaks of the phase height fluctuations provides ameasure of the Burnt-Vaisala frequency near the radio reflection height. The statistical properties of the CW doppler sounding at variable transmitting frequencies can be used to monitor certain physical parameters of the upper mesosphere and lower thermosphere.

There are no three dimensional observations of TIDs which provide information on wave front tilts and true phase velocities. The NASA/MSFC doppler sounder array data on the three dimensional TIDs and may be used to investigate wave characteristics seasonal and diurnal variations of the travelling ionospheric disturbances.

REFERENCES

Baker, D. M. and K. Davies, "Waves in the Ionosphere Produced by Nuclear Explosions," J. Geophys. Res. 73, 448, 1968.

Baker, D. M., N. Chang, K. Davies, R. Donnelly, and J. Jones, "A Review of Some Ionospheric Studies Based on a High Frequency Doppler Technique," ESSA-ERL 78-SDL-1, Washington, D. C. 1969.

Baker, D. C. and J. A. Gledhill, "An Unusual Travelling Disturbance in the F-region of the Ionosphere," J. Atmosph. Terr. Phys. 27, 1223, 1965.

Blackman, R. B. and J. W. Tukey, "The Measurement of Power Spectra," Dover Publications, Inc. New York, 1959.

Bowman, G. G., "Travelling Disturbances Associated with Ionospheric Storms," J. Atmosph. Terr. Phys. 27, 1247, 1965.

Bowman, G. G., "Extremely Large Travelling Ionospheric Disturbances in Antarctica," Scientific Report, AVCO Missile, Space and Electronics Group, 1968.

Bramley, E. N., "Direction Finding Studies of Large Scale Ionospheric Irregularities," Proc. Roy. Soc. (Lond) 220, 39, 1953.

Bramley, E. N. and W. J. Ross, "Measurements of Direction Arrival of Short Radiowaves Reflected at the Ionosphere," Proc. Roy. Soc. (Lond), 207, 252, 1951.

Castle, F. and J. M. Faynot, "Some Irregularities Observed Simultaneously in the Ionosphere at Middle Latitudes," Nature, 204, 984, 1964.

Champion, K. S. W., "Neutral Atmospheric Temperature Variations," Space Research VII, 1101, North Holland Pub., Amsterdam, 1967.

Chan, K. L. and O. G. Villard, Jr., "Observations of Large Scale Travelling Ionospheric Disturbances by Spaced Path High Frequency Measurements," J. Geophys. Res., 67, 973, 1962.

Davies, K., "Doppler Studies of the Ionosphere with Vertical Incidence," Proc. IRE 50, 94, and Proc. IRE 50, 1544, 1962.

Davies, K. and D. M. Baker, "On Frequency Variations of Ionospherically Propagated HF Radio Signals," Radio Science 1 , 545, 1966.

Davies, K., D. M. Baker and N. J. F. Chang, "Comparison Between Formulas for Ionospheric Radio Propagation and Atmospheric Wave Propagation," Radio Science 4, 231, 1969.

Davies, K., and J. E. Jones, "Three Dimensional Observations of Travelling Ionospheric Disturbances," J. Atmosph. Terr. Phys. 33, 39, 1971.

Davies, K., and J. E. Jones, "Evidence for Waves and Winds in the Ionospheric F-Region," Space Research XII, Akademic-Verlag,Berlin, 1972, p. 1149.

Davis, M. J. and A. V. da Rosa, "Travelling Ionospheric Disturbances Originating in the Auroral Oval During Polar Substorms," J. Geophys. Res., 74, 5721, 1969.

Elkins, T. J. and F. F. Slack, "Observations of Travelling Ionospheric Disturbances Using Stationary Satellites," J. Atmosph. Terr. Phys. 31, 421, 1963.

Flock, W. L. and R. D. Hunsucker, "The Auroral Zone as a Source of Travelling Ionospheric Disturbances," Proc. ESSA/ARPA Acoustic Gravity Wave Symposium ESSA, Boulder, Colorado, U.S.A., 1968, p. 159.

Friedman, J. P., "Propagation of Internal Gravity Waves in a Thermally Stratified Atmosphere," J. Geophys. Res. 71, 1033, 1966.

Georges, T. M., "Ionospheric Effects of Atmospheric Waves," ESSA Tech. Report IER 57-ITSA 54, Washington, D. C. 1967.

Georges, T. M., "HF Doppler Studies of Travelling Ionospheric Disturbances," J. Atmosph. Terr. Phys., 30, 735, 1968.

Goodwin, G. L., "Some Horizontally Moving Ionospheric Irregularities at High Latitudes," Planet. Space Sci. 16, 273, 1968.

Heisler, L. H., "Observations of Movement of Perturbation in the F-Region," J. Atmosph. Terr. Phys. 25, 71, 1963.

Hines, C. O., "Internal Atmospheric Gravity Waves at Ionospheric Heights," Cand. J. Phys. 38, 1441, 1960.

Hines, C. O., "Some Consequences of Gravity Wave Critical Layers in the Upper Atmosphere," J. Atmosph. Terr. Phys. 30, 837, 1968.

Hooke, W. H., "Ionospheric Irregularities Produced by Internal Atmospheric Gravity Waves," J. Atmosph. Terr. Phys. 30, 795, 1968.

Hunsucker, R. D. and L. H. Tveten, "Large Travelling Ionospheric Disturbances Observed at Middle Latitudes Utilizing High Resolution H. F. Backscatter Technique," J. Atmosph. Terr. Phys. 29, 909, 1967.

King, G. A. M., "The Ionospheric Disturbances and Atmospheric Waves," J. Atmosph. Terr. Phys. 28, 957, 1966.

Klostermeyer, J. A., "Gravity Waves in the F-Region," J. Atmosph. Terr. Phys. 31, 25, 1969.

Liszka, L. and G. N. Taylor, "A Synoptic Study of Large Scale Ionospheric Irregularities Using Observations of Faraday Rotation of Satellite Signals," J. Atmosph. Terr. Phys. 27, 843, 1965.

Maeda, K. and J. M. Young, "Propagation of Pressure Waves Produced by Auroras," J. Geomag. Geoelec. 18, 275, 1966.

Munro, G. H., "Travelling Disturbances in the Ionosphere," Proc. Roy. Soc. (Lond.) 202, 208, 1950.

Munro, G. H., "Reflections from Irregularities in the Ionosphere," Proc. Roy. Soc. (Lond.) A219, 447, 1953.

Munro, G. H., "Travelling Ionospheric Disturbances in the F-Region of the Ionosphere," Aust. J. Phys. 11, 91, 1958.

Price, R. E., "Travelling Ionospheric Disturbances in the Ionosphere," Nature, 172, 115, 1953.

Price, R. E., "Travelling Disturbances in the Ionosphere," Physics of the Ionosphere, Phys. Soc. (Lond.) 181, 1955.

Rao, G. L., "Models of Gravity Wave Perturbations of the Neutral Upper Atmosphere of the Earth," NASA CR 2033, 1972.

Reddi, C. R. and B. R. Rao, "Characteristics of Travelling Ionospheric Perturbations over Waltair Using Phase Path Technique," J. Atmosph. Terr. Phys. 33, 251, 1971.

Thomas, L., "Some Measurements of Horizontal Movements in F2 Region Using Widely Spaced Observing Stations," J. Atmosph. Terr. Phys. 14, 123, 1959.

Thome, G. D., "Incoherent Scatter Observations of Travelling Ionospheric Disturbances," J. Geophys. Res. 69, 4047, 1964.

Thome, G. E., "Long Period Waves Generated in the Polar Ionosphere During the Onset of Magnetic Storms," J. Geophys. Res., 73, 6319, 1968.

Tilteridge, J. E., "Periodic Disturbances in the Ionosphere," J. Geophys. Res. 73, 243, 1968.

Tolstoy, I., "The Theory of Waves in Stratified Fluids Including the Effects of Gravity and Rotation," Rev. Mod. Phys. 35, 207, 1963.

Tolstoy, I., and H. Montes, "Phase Height Fluctuations in the Ionosphere Between 130-250 km," J. Atmosph. Terr. Phys. 33, 775, 1971.

Vasseur, G. and P. Waldteufel, "Thomson Scatter Observations of Gravity Waves in the Ionospheric F-Region," J. Atmosph. Terr. Phys. 31, 885, 1969.

Wilson, C. R., "Auroral Infrasonic Waves," J. Geophys. Res. 74, 1812, 1969.

Wright, M. D., "Possible Identification of Atmospheric Waves Associated with Ionospheric Storms," Nature 190, 898, 1961.

Wu, S. T., R. J. Hung, G. L. Rao, and R. E. Smith, "Wind Shear Effect on Acoustic-Gravity Wave Propagation in the Thermosphere," submitted to J. Atmosph. Sciences, 1974.

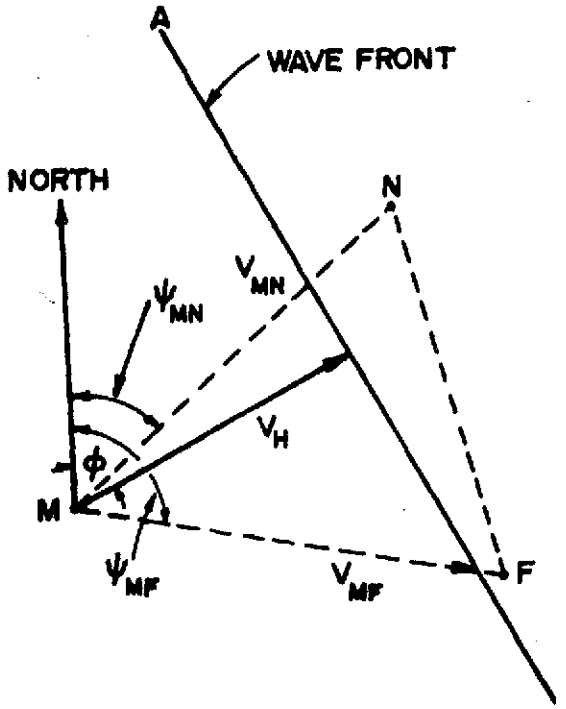

Figure 1 Graphical representation of wave front moving across the doppler sounder array.

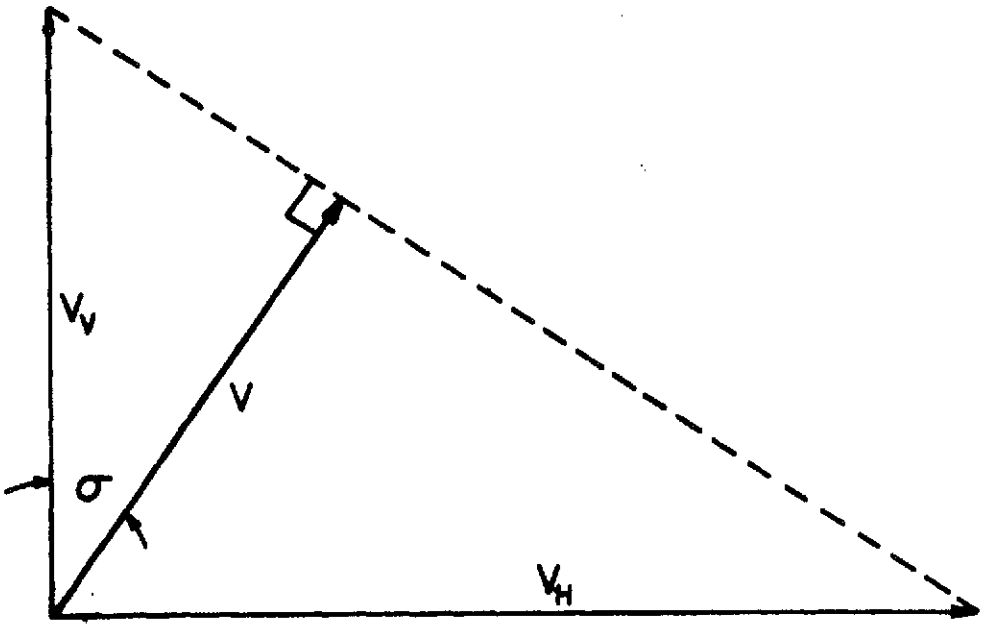

Figure 2 Graphical representation for computing phase velocity of the wave front.

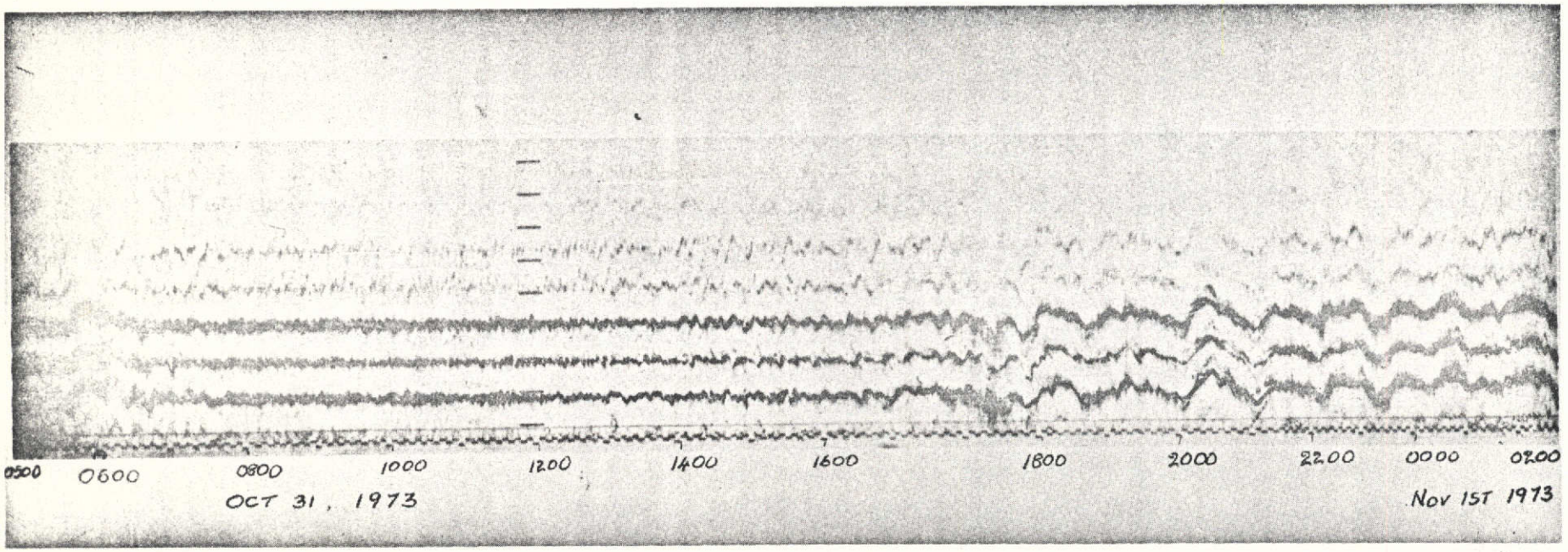

Figure 3. Typical 24 hour doppler record taken at 4.080 MHz operating frequency.

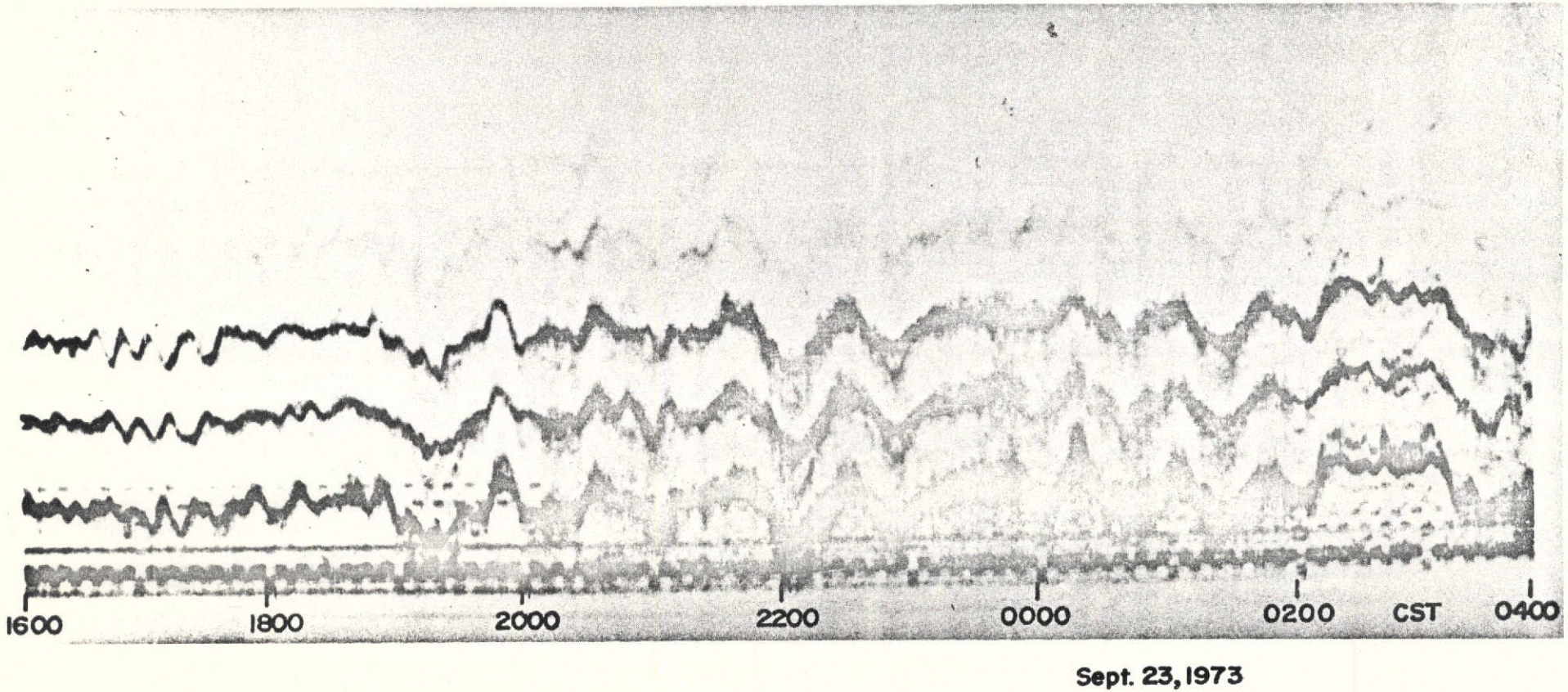

Figure 4a. Typical TID observed on Sept. 23, 1973, on 4.080 MHz operating frequency.

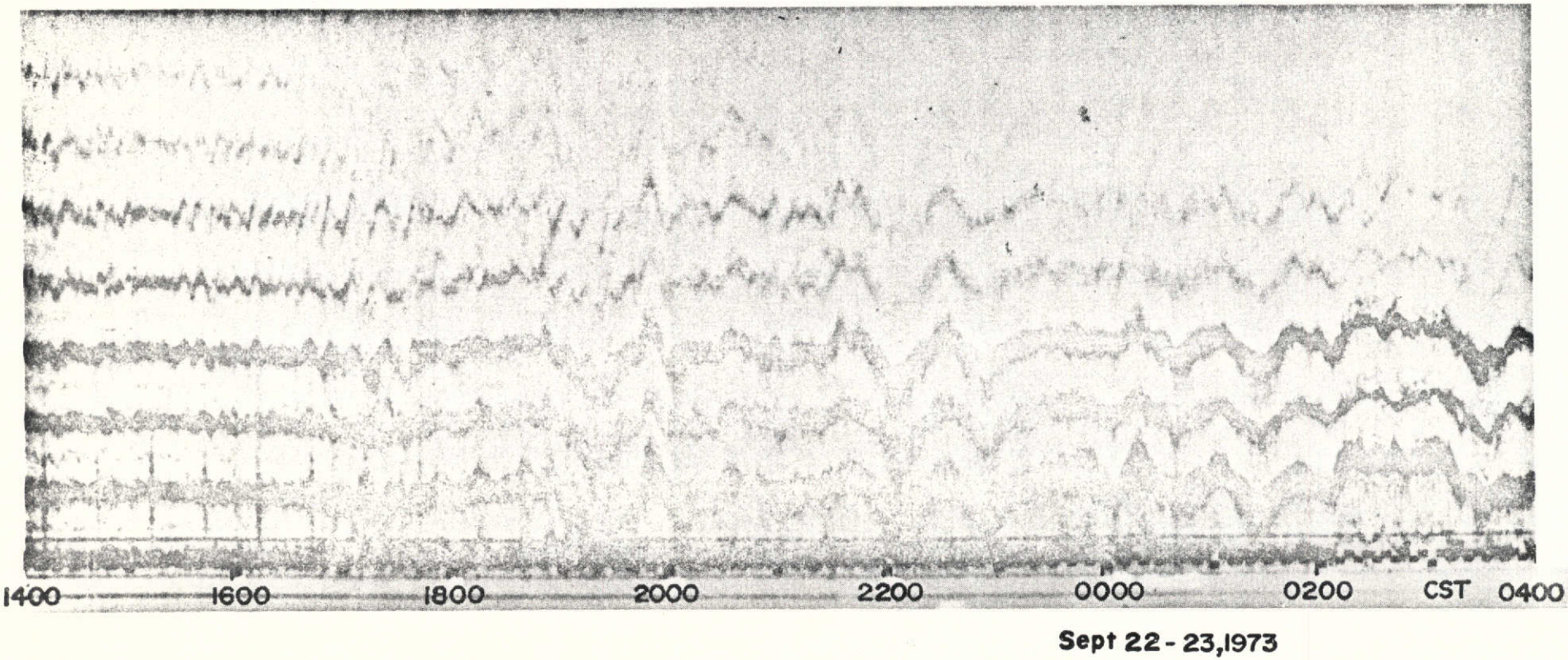

Figure 4b. Typical TID observed on Sept. 23, 1973, on 4.759 MHz operating frequency.

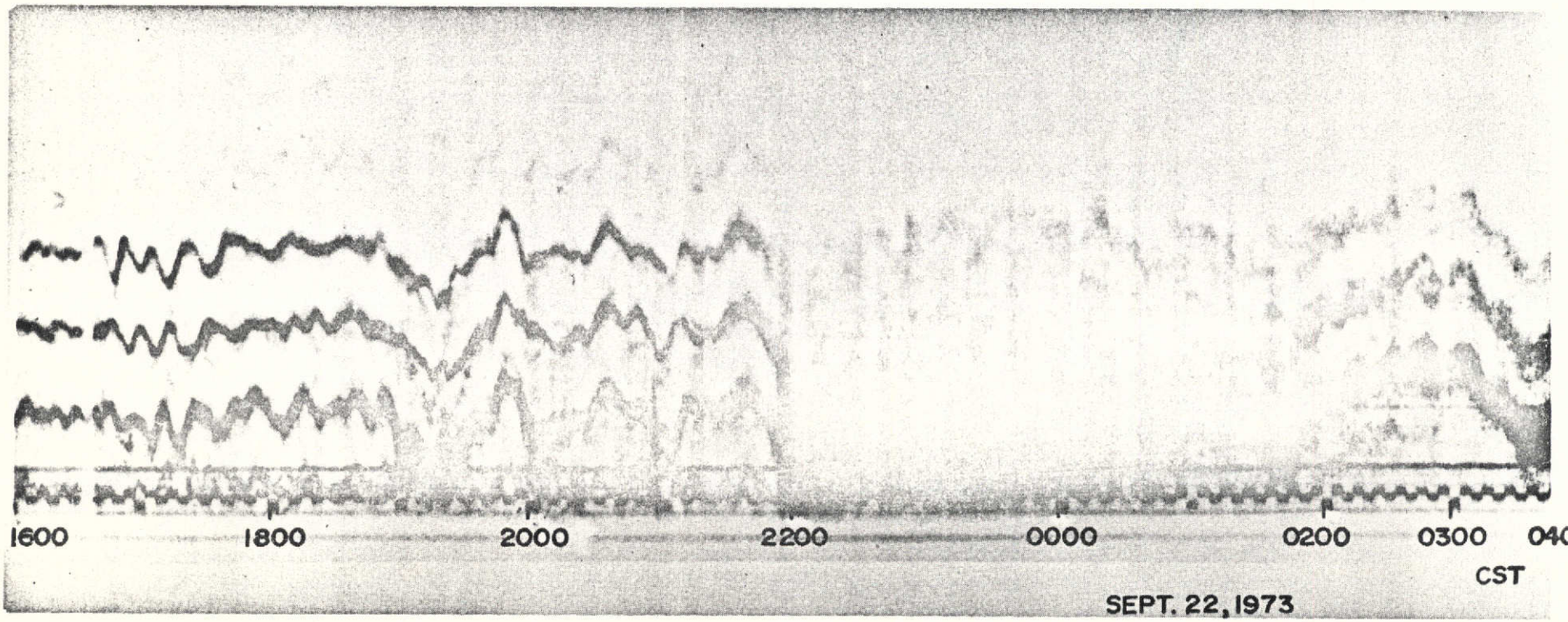

Figure 4c. Typical TID observed on Sept. 23, 1973, on 5.734 MHz operating frequency.

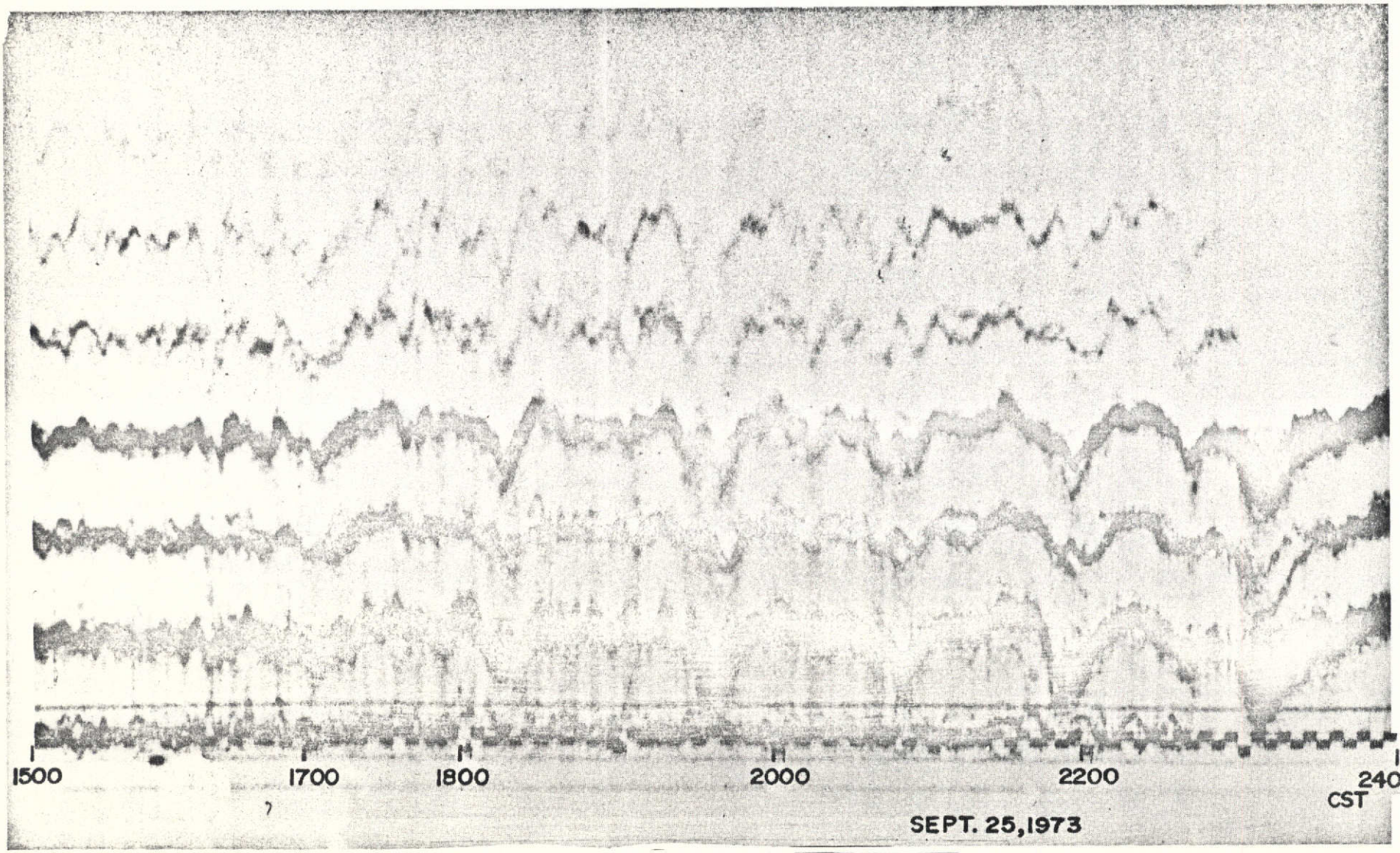

Figure 5a. Typical TID observed on Sept. 25, 1973, on 4.080 MHz operating frequency.

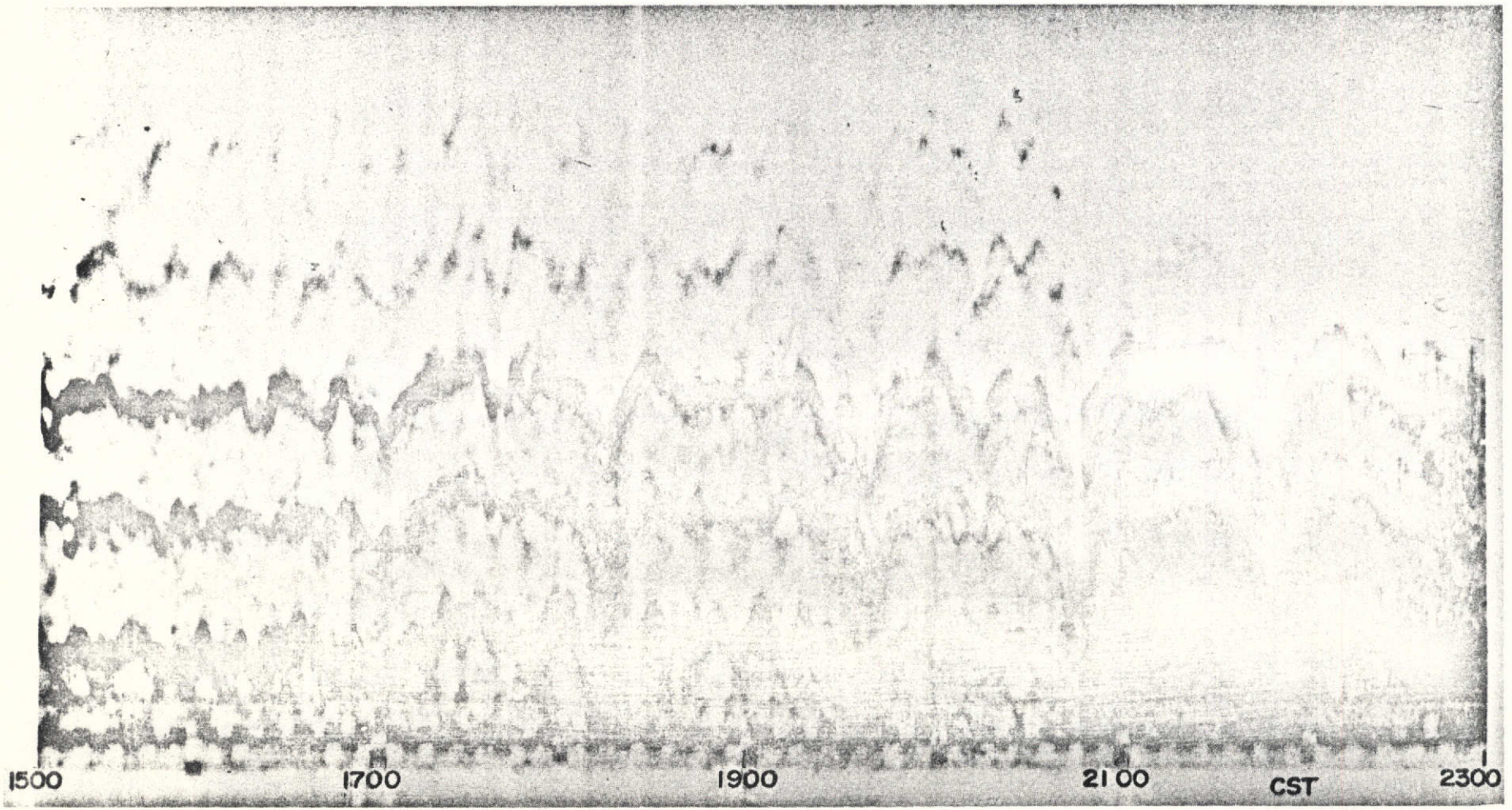

Figure 5b. Typical TID observed on Sept. 25, 1973, on 4.759 MHz operating frequency.

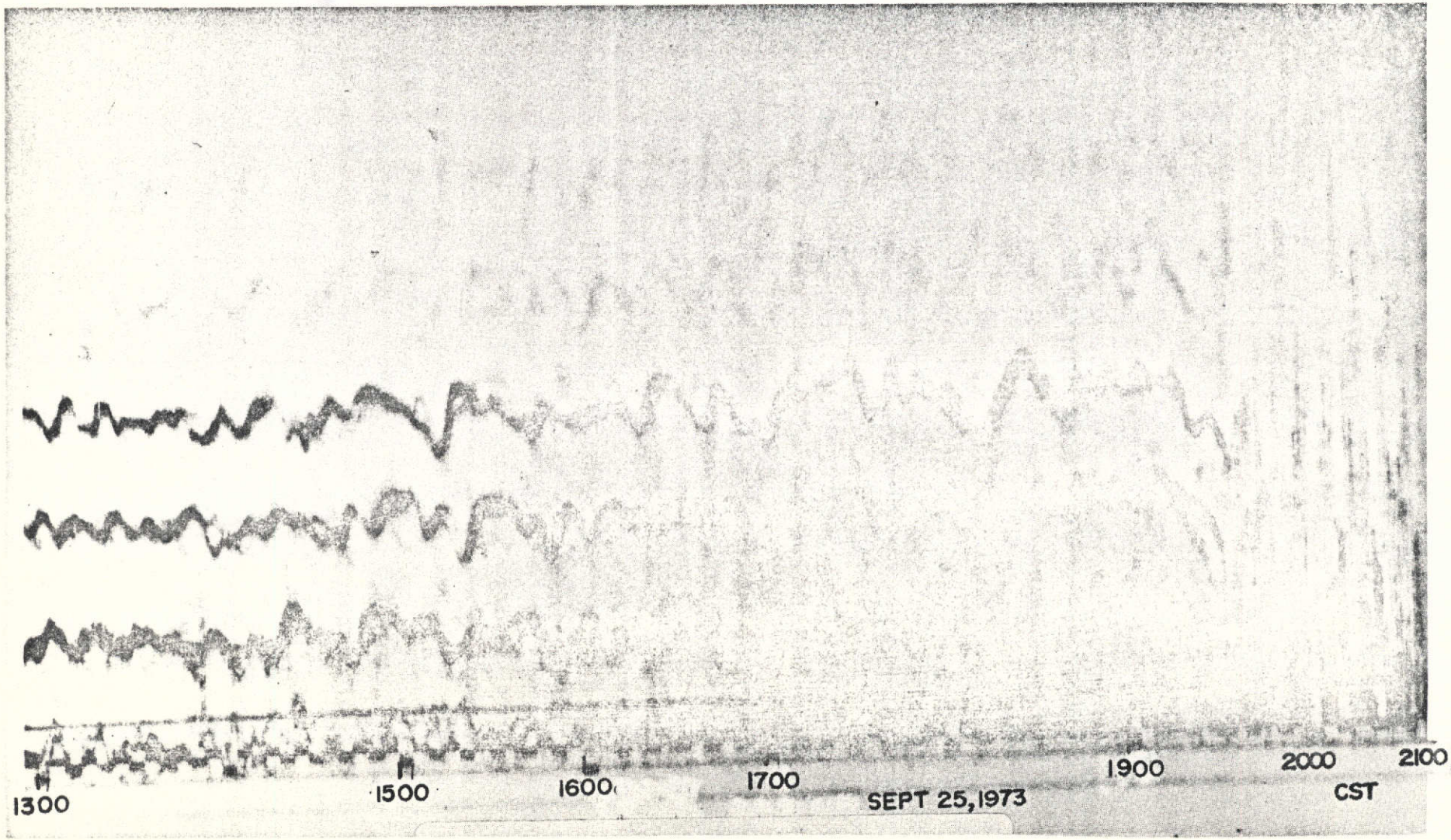

Figure 5c. Typical TID observed on Sept. 25, 1973, on 5.734 MHz operating frequency.

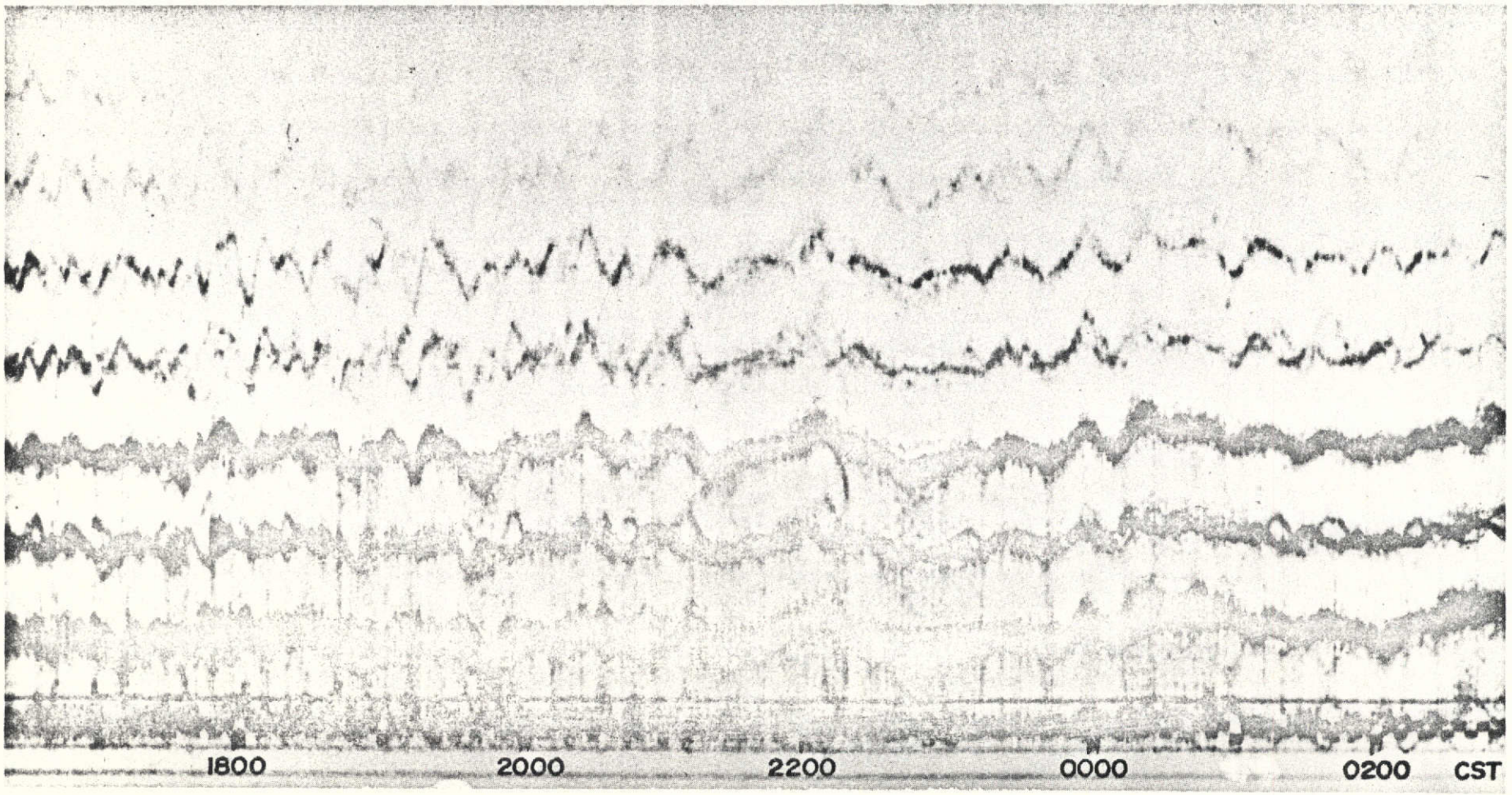

Figure 6a. Typical TID observed on Oct. 1, 1973, on 4.080 MHz operating frequency.

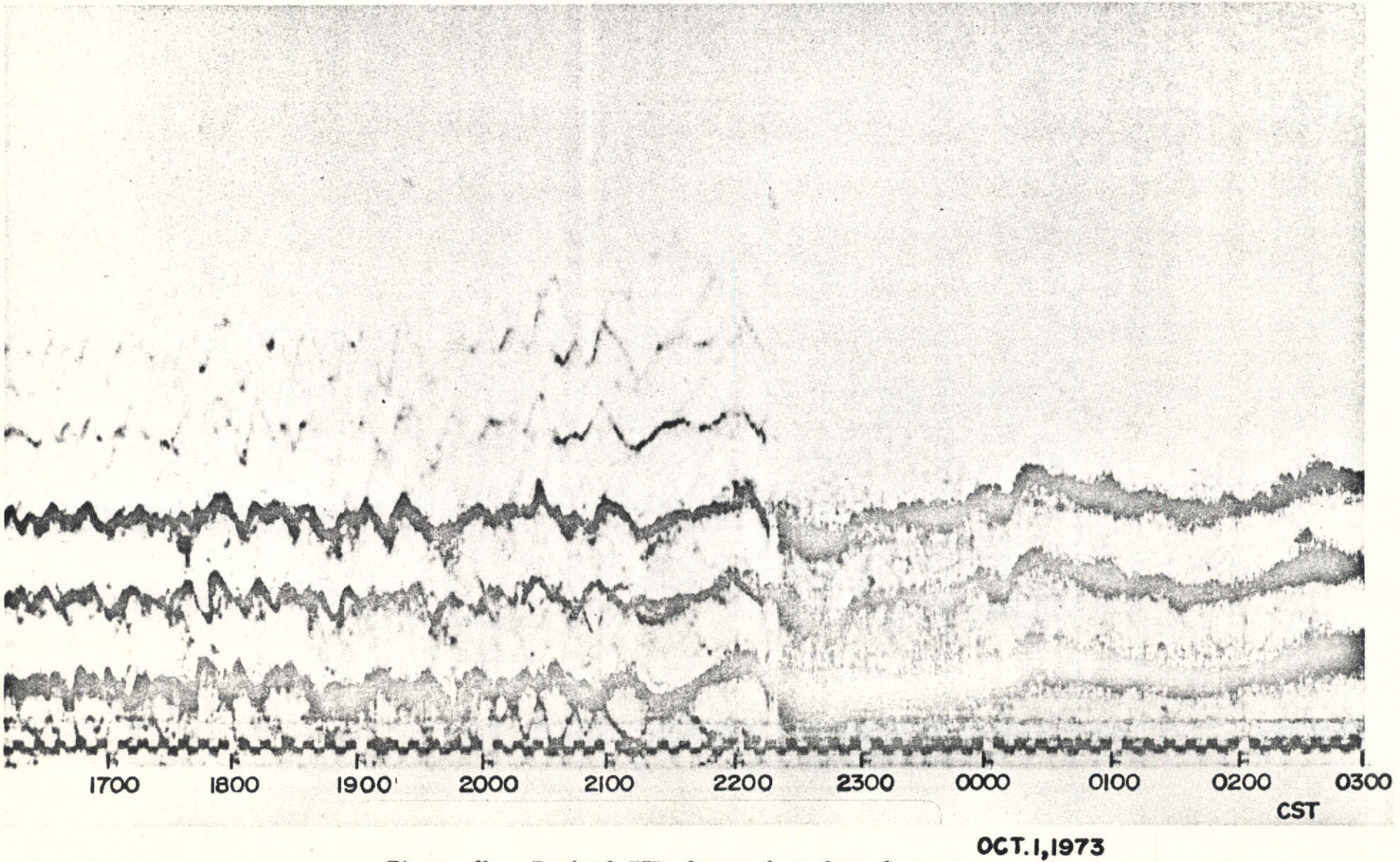

Figure 6b. Typical TID observed on Oct. 1, 1973, on 4.759 MHz operating frequency.

Figure 6c. Typical TID observed on Oct. 1, 1973, on 5.734 MHz operating frequency.

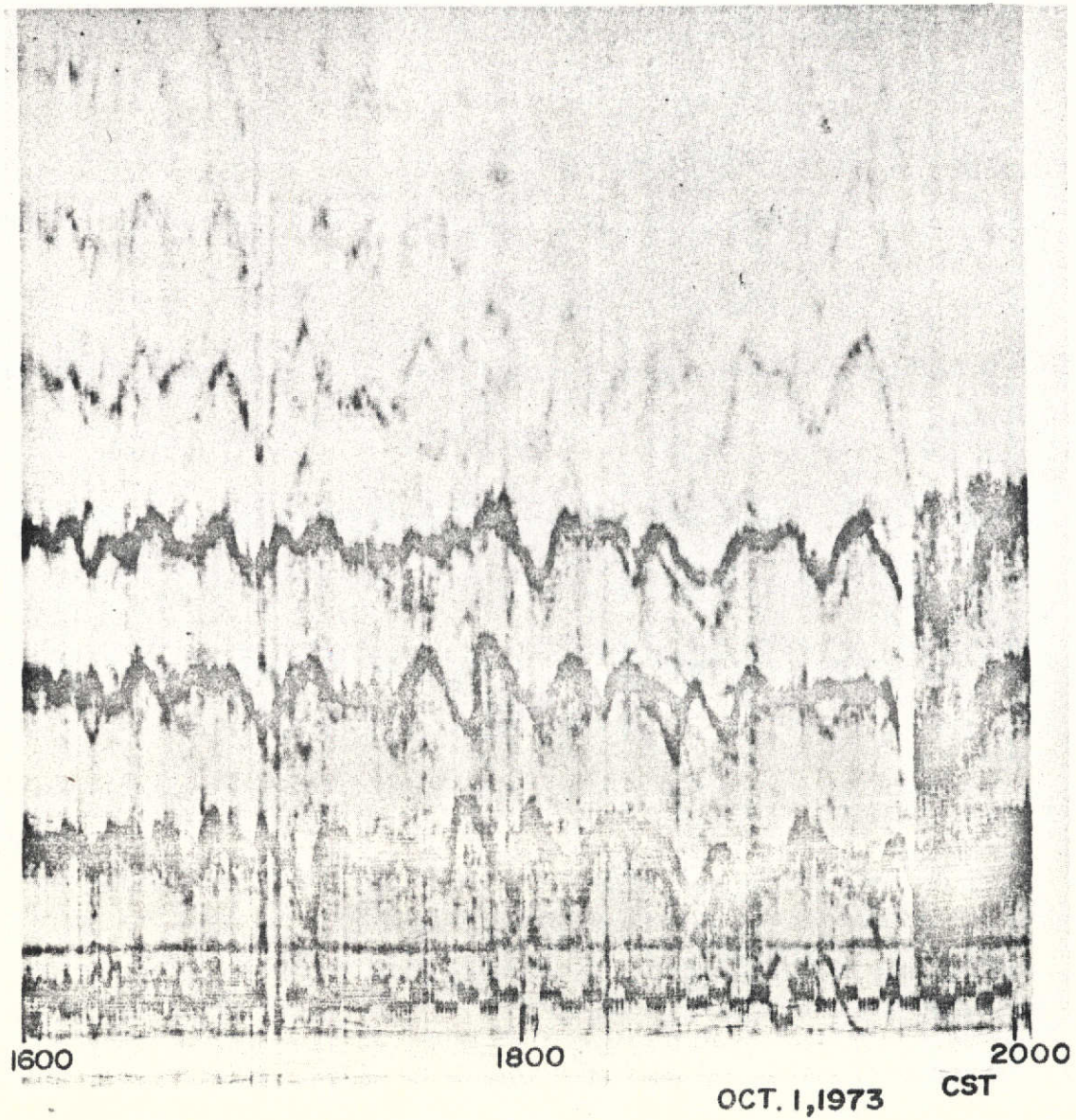

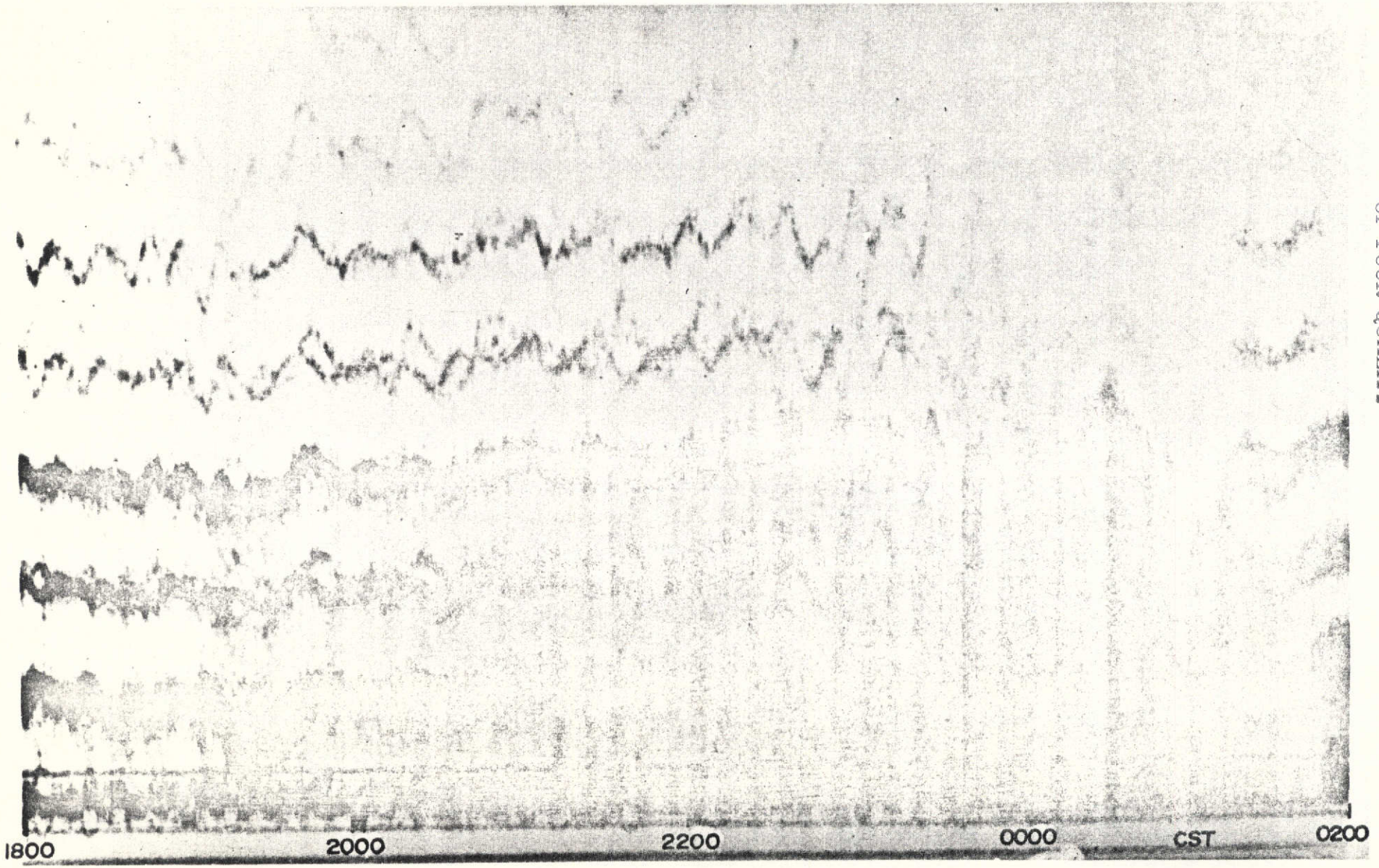

Figure 7a. Typical TID observed on Oct. 2, 1973, on 4.080 MHz operating frequency.

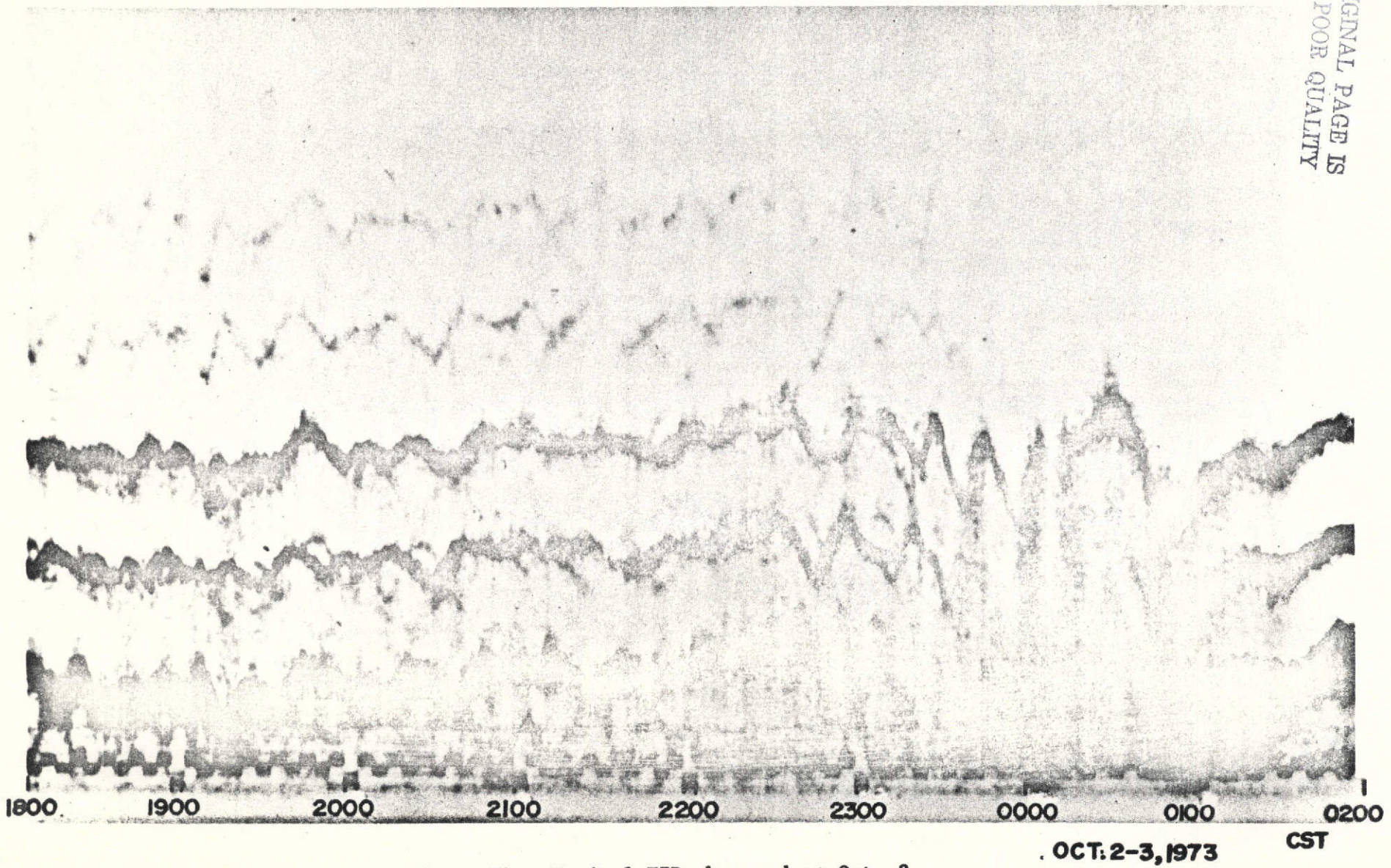

Figure 7b. Typical TID observed on Oct. 2, 1973, on 4.759 MHz operating frequency.

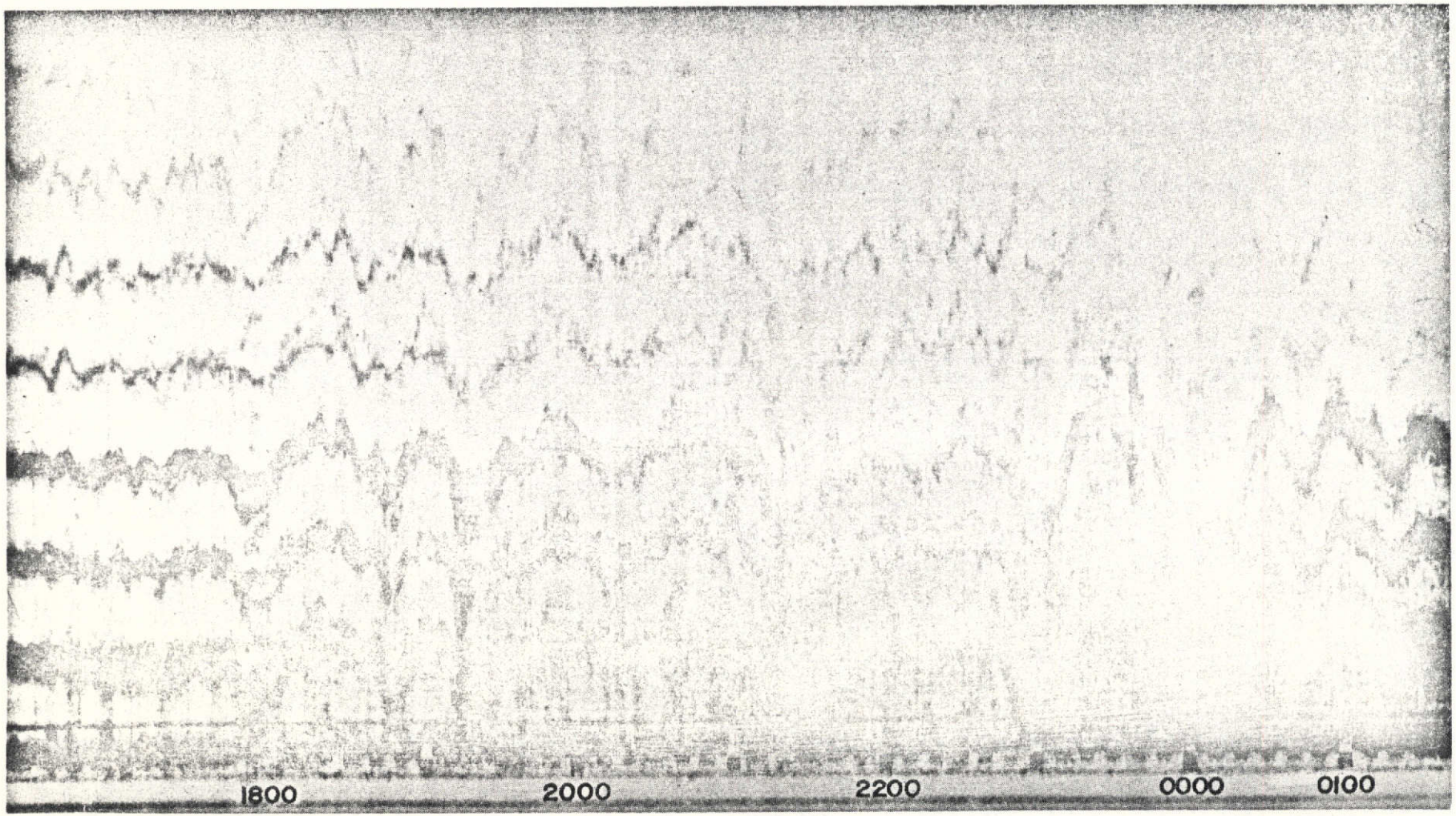

Figure 8a. Typical TID observed on Oct. 3, 1973, on 4.080 MHz operating frequency.

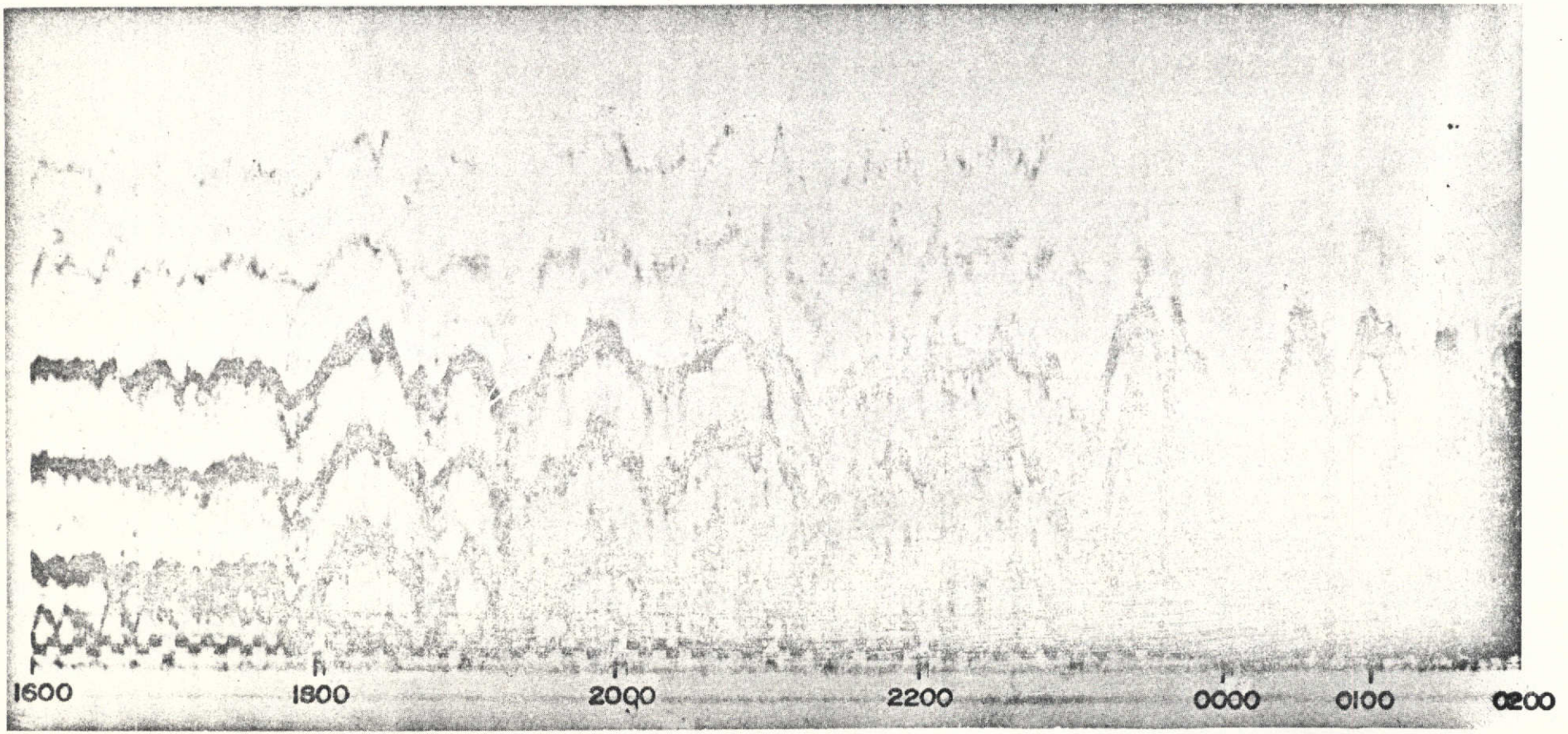

Figure 8b. Typical TID observed on Oct. 3, 1973, on 4.759 MHz operating frequency.

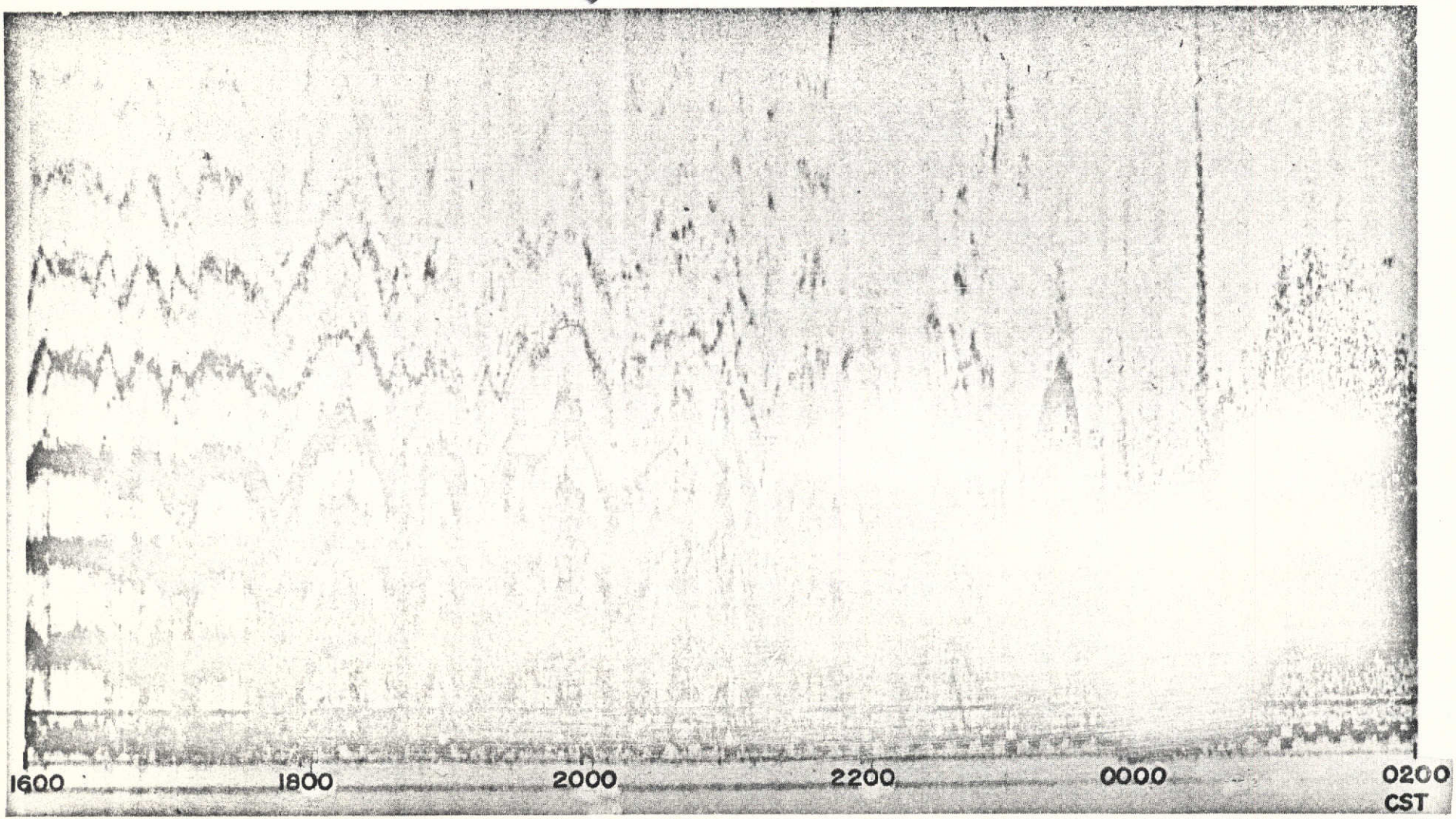

Figure 8c. Typical TID observed on Oct. 3, 1973, on 4.734 MHz operating frequency.

Figure 9. Diunal variation of TID phase speeds in winter.

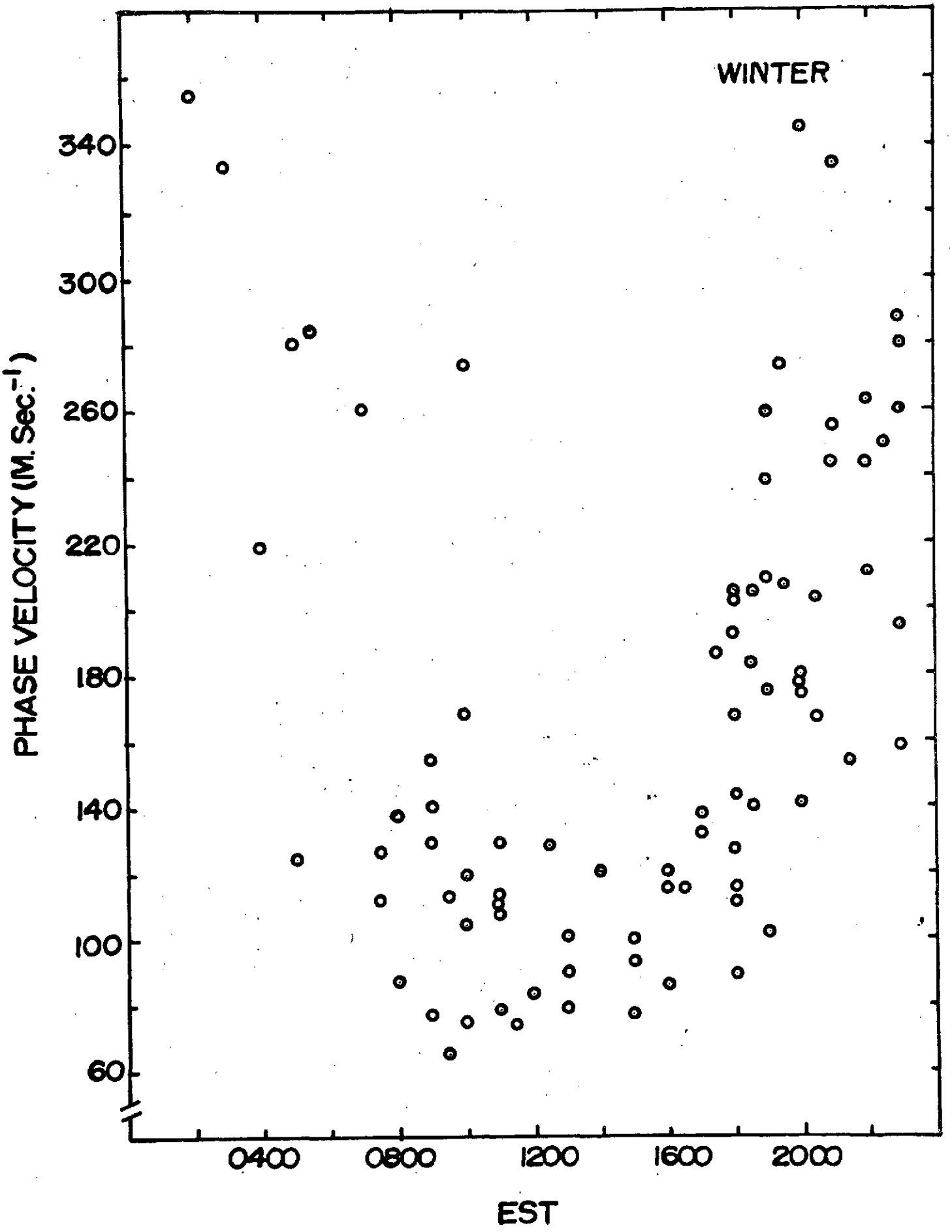

Figure 10. Diunal variation of TID phase speeds in equinox.

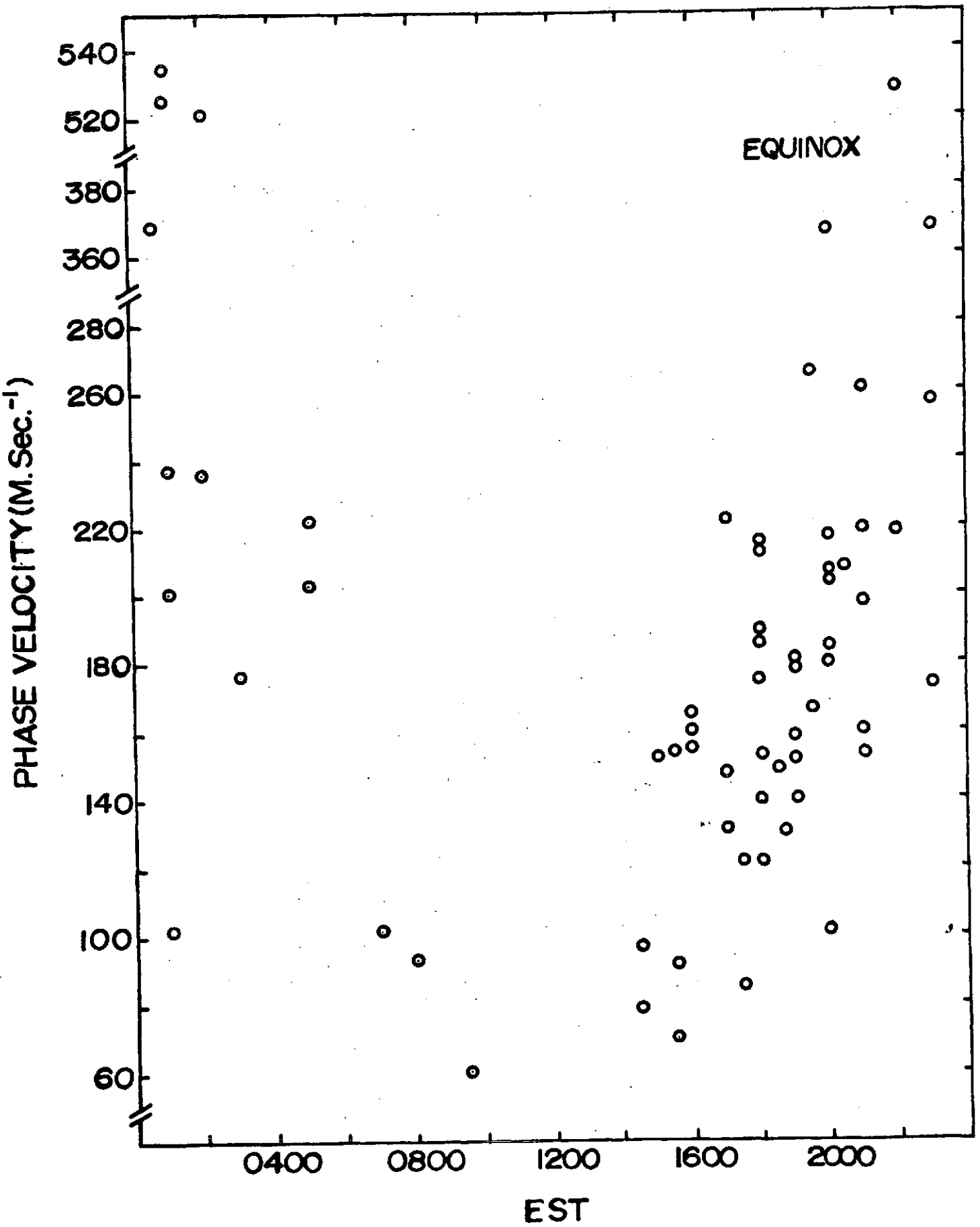

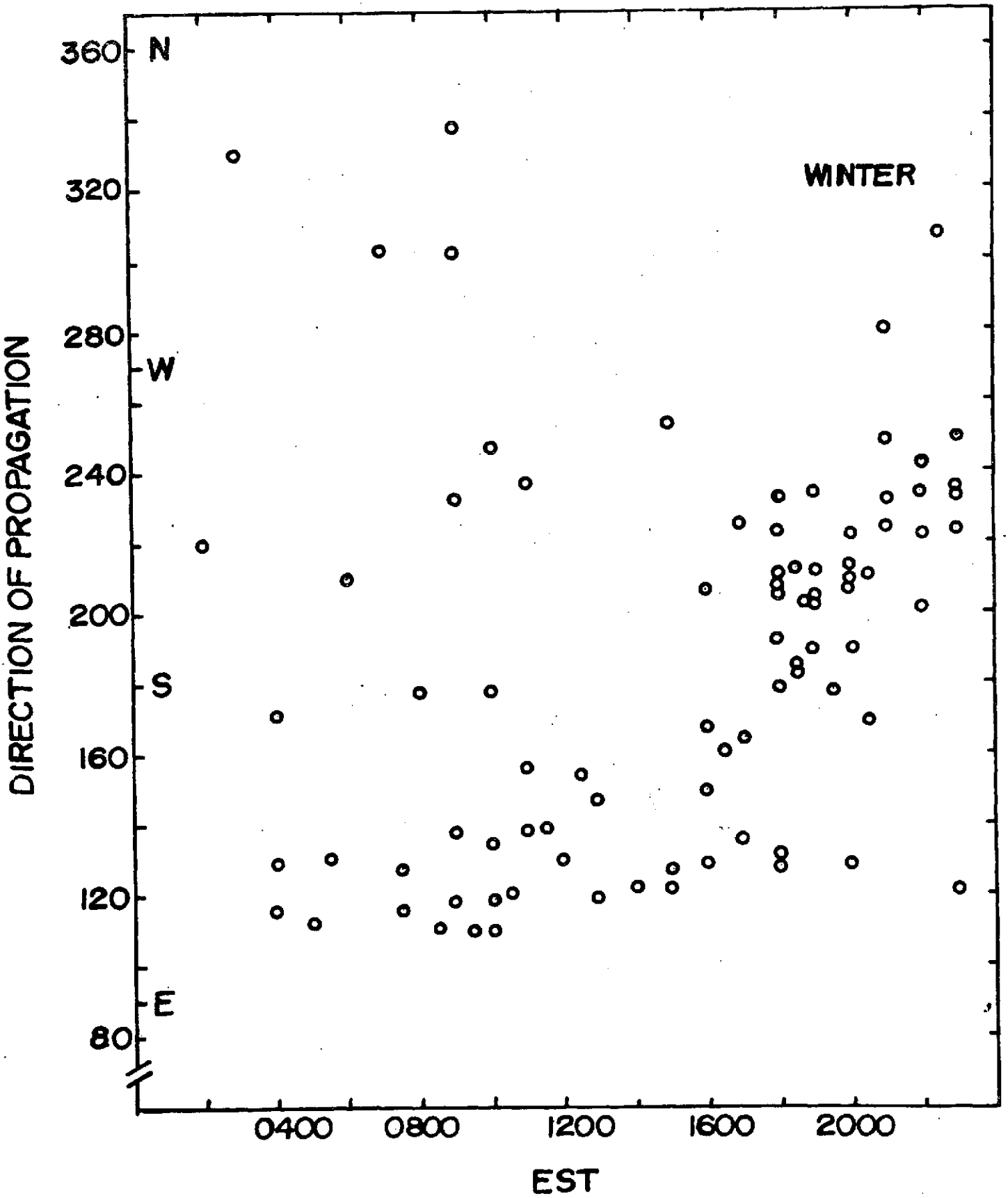

Figure 11. Diunal variation of TID direction of propagation in winter.

Figure 12. Diunal variation of TID direction of propagation in equinox.

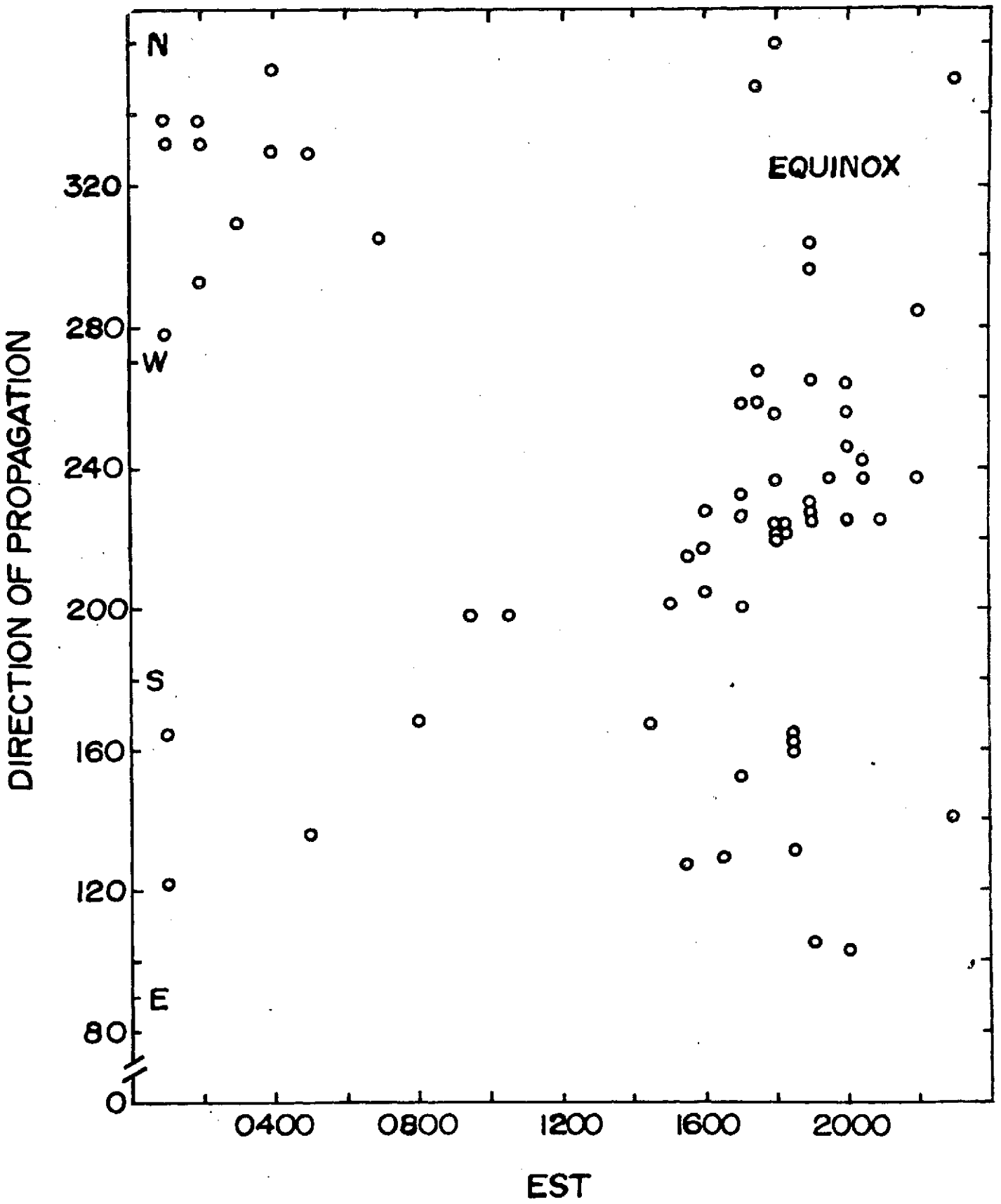

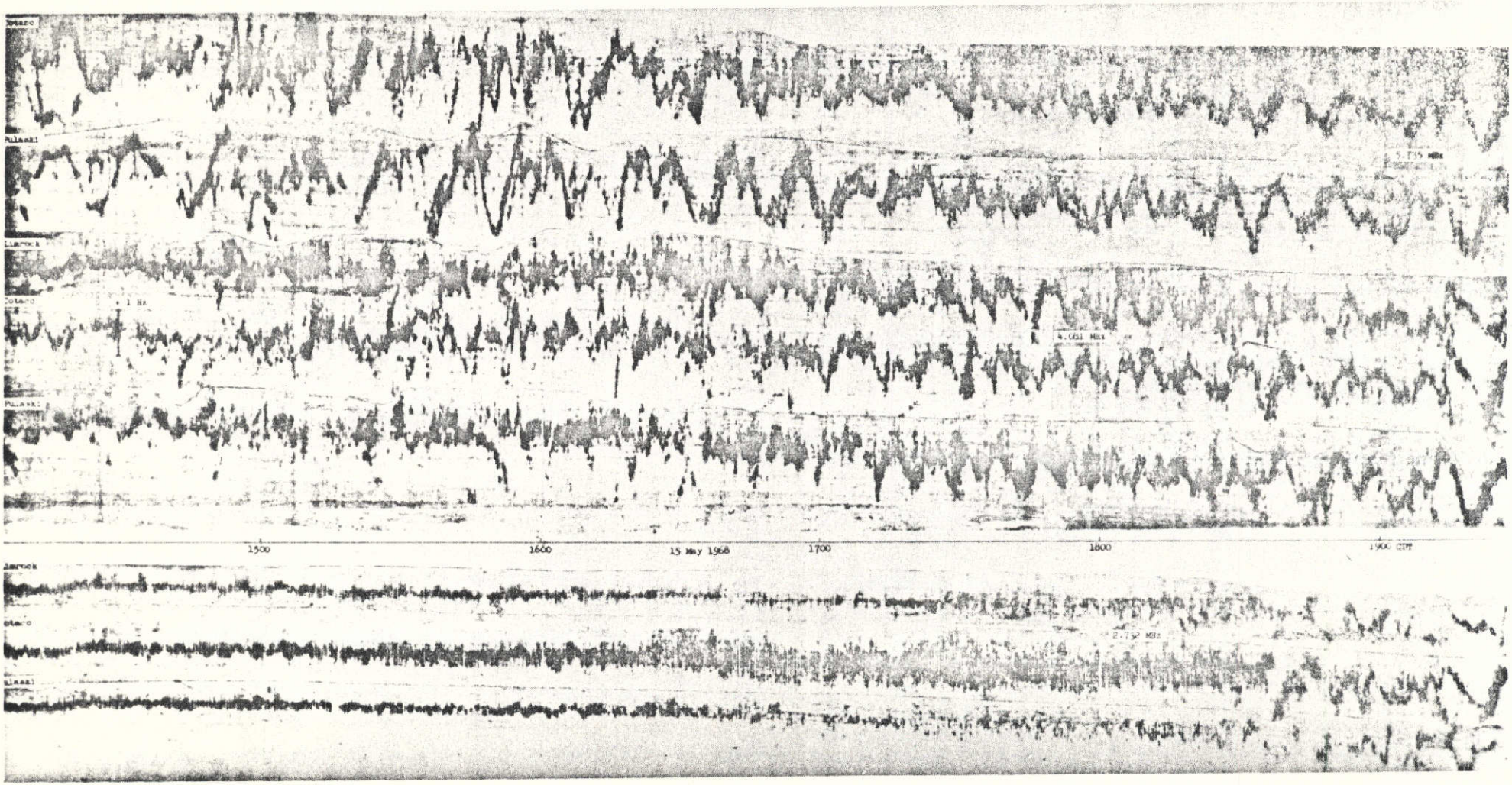

Figure 13. CW Doppler record showing the thunder storm correlated doppler fluctuations.

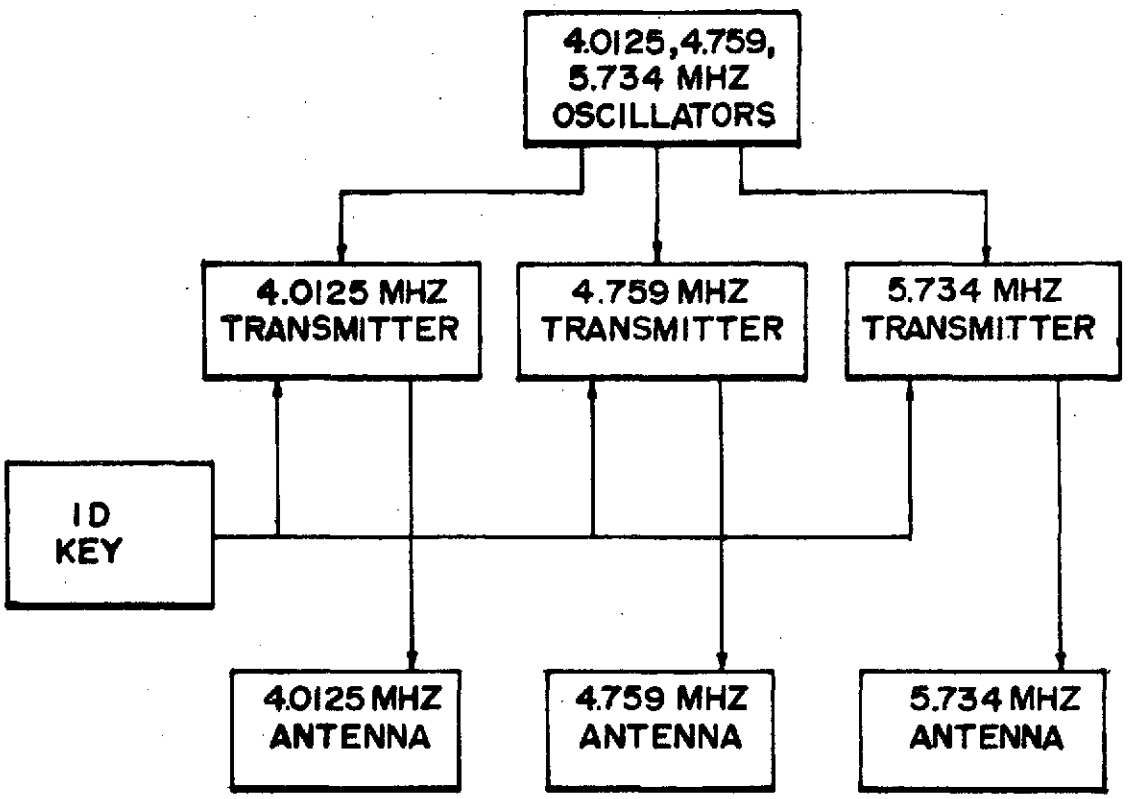

Figure 14. Block diagram of transmitting system.

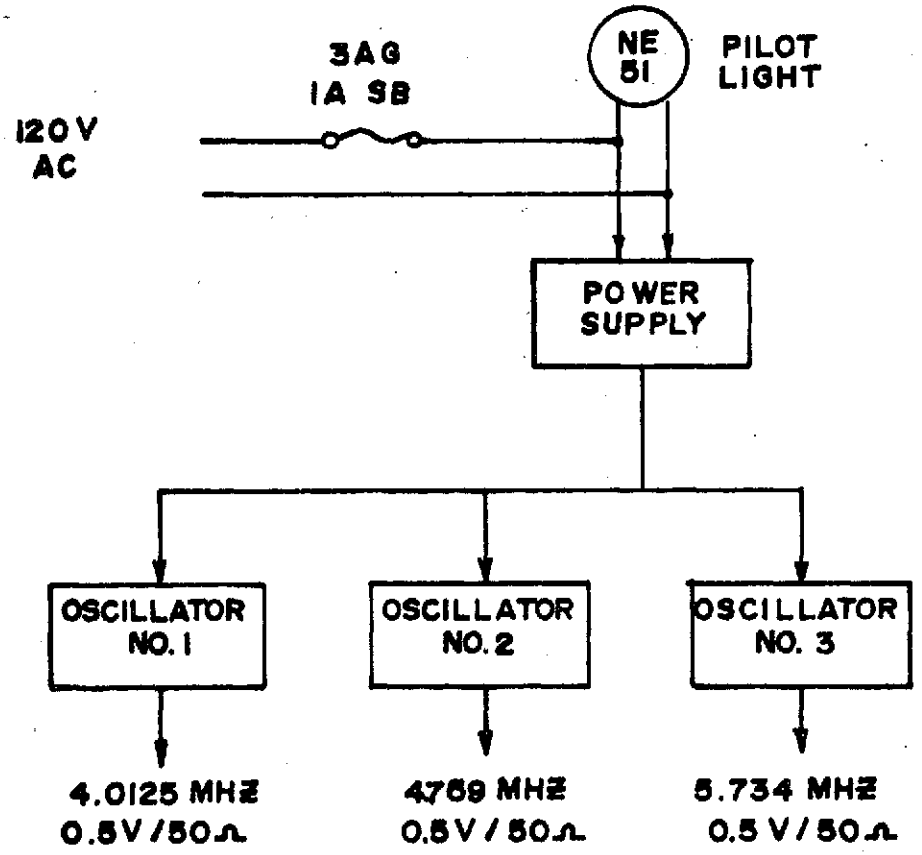

Figure 15. Block diagram of Oscillator chasis.

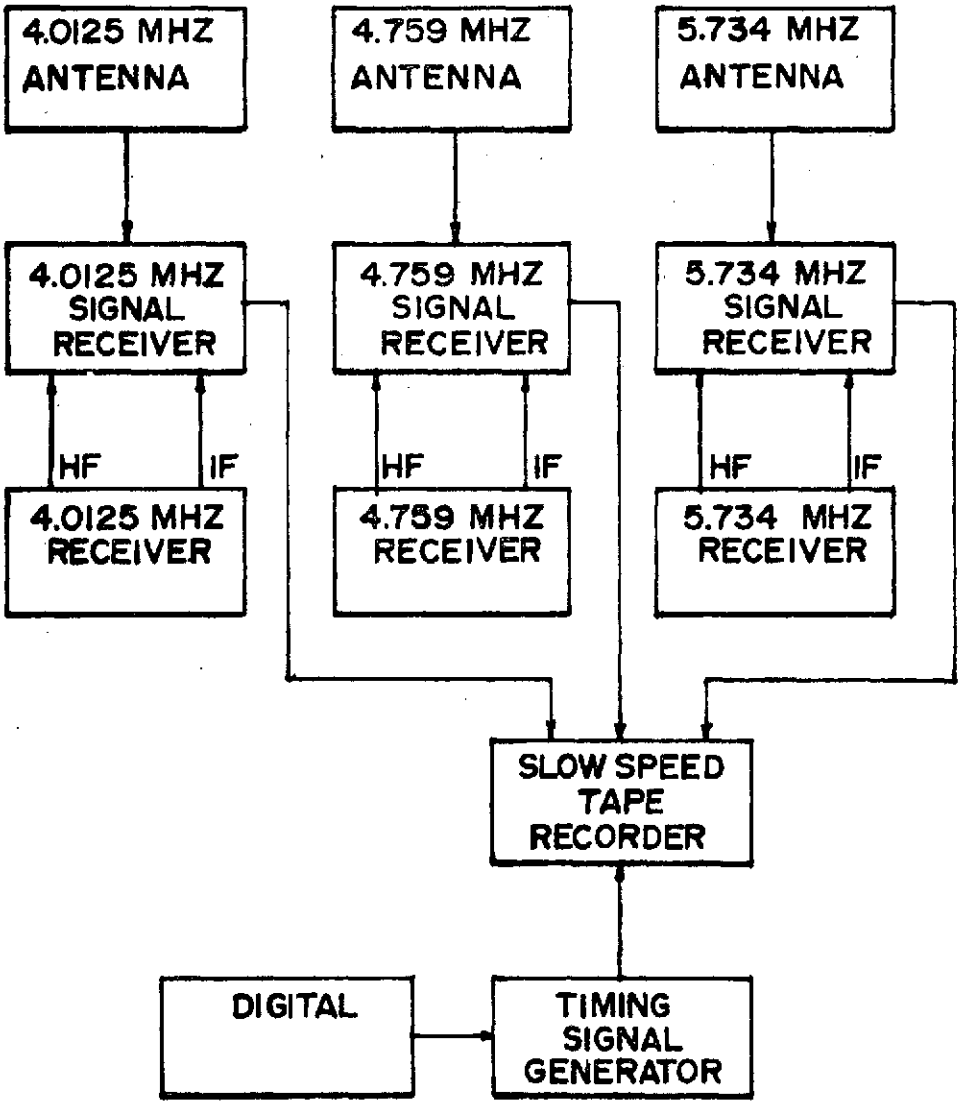

Figure 16. Block diagram of receiving system.

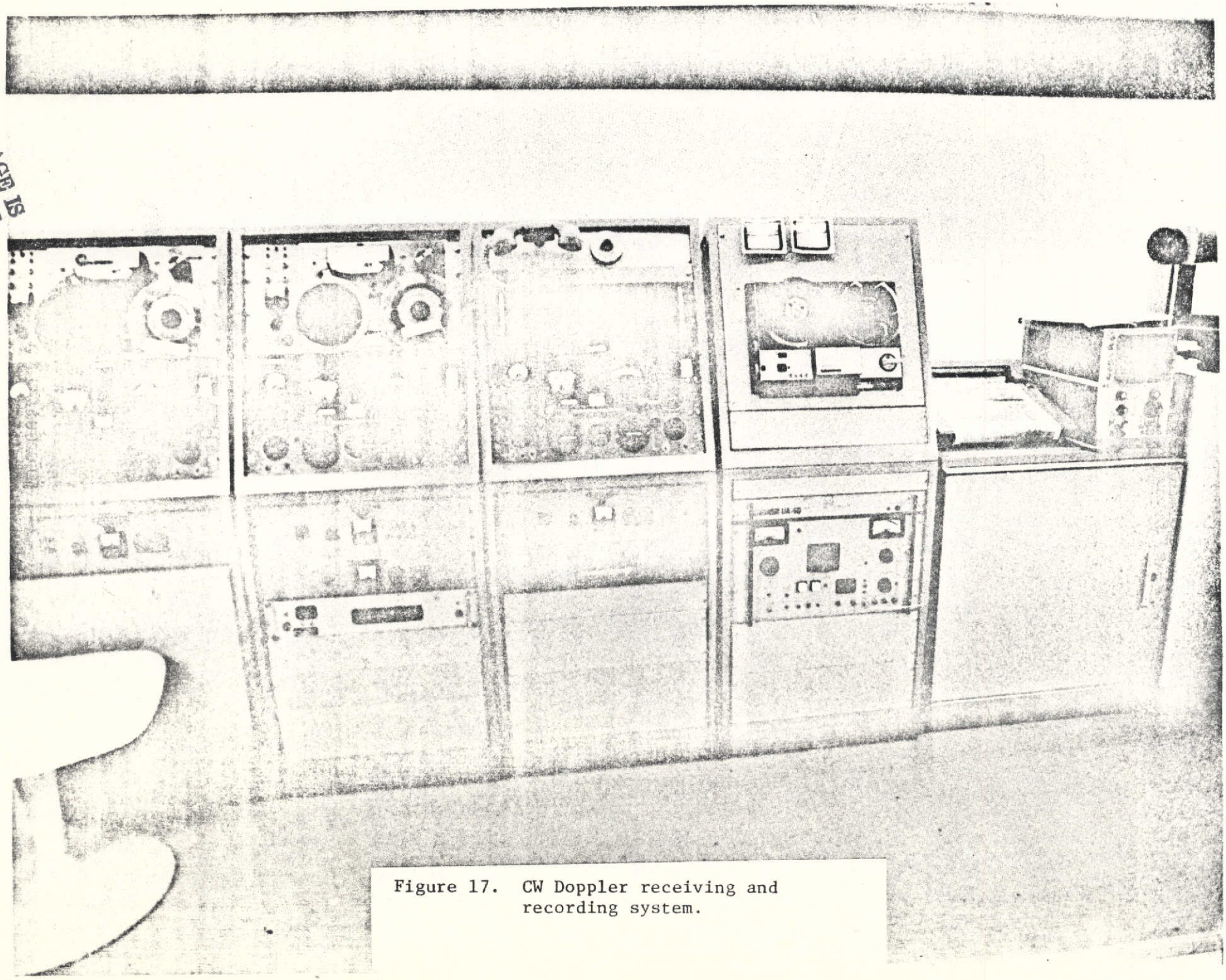

Figure 17. CW Doppler receiving and recording system.

TABLE 1

PHASE-PATH SOUNDER EQUIPMENT CHARACTERISTICS

1. **Transmitter Power Output:** 2.5 kw peak emitted power

2. **Frequency Range:** 2 to 26 MHz, stepped manually or programmed (2 channels only)

3. **Programmed Frequency Steps:**
   Selectable: 1, 10, 20 40 or 100 KHz steps per prf, 2, 4, 8 or 16 prf.

4. **Pulse Repetition Rates:** 20 or 40 per second per channel. Maximum of 4 channels available (Sequential pulsing is used).

5. **Pulse Width:** **Selectable:** 100, 200, 300 or 500 microseconds
   Selectable: Square or Gaussian pulse

6. **Recorded Data:** Digitally processed for magnetic tape, two programmed receiver channels of:
   a. Pulse group delay (1 microsecond resolution) 14 bits (τ)
   b. Pulse phase delay (3.6 degree resolution) 7 bits (ϕ)
   c. End of block frequency 16 bits each channel
   d. Julian day 16 bits
   e. Time of day (hour-minute-second) 24 bits
   f. Parity check for items (1) and (2) above
   g. Data recorded in blocks of 600 pulse groups of group delay, phase delay, frequency, day and time. Each block consists of 4,813 bytes (4,812 6-bit bytes equals 3,609 8-bit words pulse one 6-bit longitudinal parity check word).

7. **Processed real-time delay:** Two programmed receiver output channels of:
   a. pulse group delay (range to 900 km .... 6 milliseconds)
   b. pulse group differential with time
   c. pulse phase ($\pm$ 180 degrees relative phase)
   d. pulse phase differential with time

   Four receiver output channels of:
   a. pulse group delay, or
   b. pulse phase ($\pm$ 180 degree relative phase), or
   c. swept frequency ionograms (two channels)

TABLE 2

FORMULAS CONNECTING THE FREQUENCY VARIATIONS

Equation and Comment	Assumptions
$\Delta f = -\frac{f}{c}\frac{dP}{dt}$ Basic Equation	Time and Space Variation of ionosphere slow compared to f (SVI)
$\Delta f \propto \frac{1}{cf} \int \frac{1}{\mu}\frac{\partial N}{\partial t} ds$	SVI Concentric ionosphere (CI) No Magnetic Field (NF) No Collisions (NC)
$\Delta f = -\frac{2fV_v}{c} \propto f$ Specular Reflection	SVI, NF Stationary Transmitter and Receiver (STR) Vertical-Incidence Propagation (VI)
$\Delta f \propto f^{-1}$ Nondeviative layer ($\mu \approx 1$)	SVI, NF, STR, NF, NC, CI
$\Delta f \propto \Delta H$ Hall Drift Model	Current flowing in the E-region produces fluctuating magnetic field at surface of Earth
$\Delta f \propto \frac{d}{dt}\Delta H$ Sudden Commencement Model	
$\Delta f \propto \Delta H f^{-1/2}$ Alfven Wave Model	
$A^2 \propto 1 - \frac{h}{2v_h^2}\frac{d^2p}{dt^2}$ $= 1 + \frac{h}{2v_h^2}\frac{c}{f}\frac{d}{dt}$	

TABLE 2 (continued)
FORMULAS CONNECTING THE FREQUENCY VARIATIONS

t = Time

f = Transmitter frequency

P = $\int \mu \cos \alpha \, ds$ phase path

α = Angle between ray path and wave normal

s = Ray-path length, measured from transmitter to point of interest

c = Speed of light, 3×10^8 m/s

N = Electron number density

μ = Refractive index given by the Appleton-Hartree equation

V = Velocity of reflecting surface. Subscripts v and h represent vertical and horizontal velocities, respectively

ΔH = Fluctuation in the horizontal component of geomagnetic field

h = Height of reflecting surface

TABLE

DISPERSION FORMULAS FOR GRAVITY WAVES AND WHISTLERS

	Gravity Wave Formulas		Whistler Wave Formulas	
Refractive index	$\mu^2 = \frac{X - 1}{Y^2 \sin^2 \psi - 1}$	(10a)	$\mu^2 = \frac{X}{\lvert Y \cos \theta \rvert - 1}$	(10b)
Limiting refractive index ($X \gg 1$, $Y \sin \psi \gg 1$)	$\mu^2 \approx \frac{X}{Y^2 \sin^2 \psi} = \frac{\omega_a^2}{\omega_g^2 \sin^2 \psi}$	(11a)	$\mu^2 \approx \frac{X}{\lvert Y \cos \theta \rvert} = \frac{\omega_N^2}{\omega \lvert \omega_H \cos \theta \rvert}$	(11b)
Critical propagation angle	$\sin \psi_{min} = 1/Y; \quad \sin \psi_{max} = -1/Y$	(12a)	$\cos \theta_{max} = 1/Y$	(12b)
Angle α between wave normal and ray (for long waves)	$\tan \alpha = -\cot \psi$	(13a)	$\tan \alpha \approx 1/2 \tan \theta$	(13b)
Group velocity for very long waves	$u = C \frac{\omega_g}{\omega_a} \sin \psi$	(14a)	$u = 2c \frac{\omega^{1/2} \omega_H^{1/2}}{\omega_N} \cos^{1/2} \theta$	(14b)

TABLE 3

COMPARISON BETWEEN ATMOSPHERIC WAVES AND MAGNETOIONIC RADIO WAVES (ISOTHERMAL ATMOSPHERE)

Acoustic Waves (isothermal atmosphere)			Radio Waves		
Acoustic cutoff frequency	$\omega_a^2 = \frac{C^2}{4H^2}$	(1a)	Plasma frequency	$\omega_H^2 = \frac{Ne^2}{\varepsilon_0 m}$	(1b)
Brunt-Vaisala frequency	$\omega_g^2 = \frac{g}{H}\left(1-\frac{1}{\gamma}\right)$	(2a)	Gyrofrequency	$\omega_H^2 = \left[\frac{e}{m} B_0\right]^2$	(2b)
	$X = \frac{\omega_a}{\omega}^2$	(3a)		$X = \left[\frac{\omega_N}{\omega}\right]^2$	(3b)
	$Y = \frac{\omega_g}{\omega}$	(4a)		$Y = \frac{\omega_H}{\omega}$	(4b)
Refractive index with gravity	$\mu^2 = \frac{C^2 k^2}{\omega^2} = \frac{1-X}{1-Y^2 \sin^2\psi}$	(5a)	Refractive index with magnetic field	$\mu^2 = \frac{c^2k^2}{\omega^2} = 1 - \frac{2X(1-X)}{2(1-X) - Y^2\sin^2\theta \pm [Y^4\sin^4\theta + 4Y^2(1-X)^2\cos^2\theta]^{1/2}}$	(5b)
Refractive index with $\omega >> \omega_g$	$\mu^2 = 1 - X$	(6a)	Refractove index with $\omega >> \omega_H$	$\mu^2 = 1 - X$	(6b)
Vertical propagation ($X < 1$)	$\mu^2 = 1 - X$	(7a)	Transverse propagation (ordinary wave)	$\mu^2 = 1 - X$	(7b)
Angle α between wave vector k and the ray	$\tan\alpha = -\frac{Y^2 \sin\psi \cos\psi}{Y^2 \sin^2\psi - 1}$	(8a)	Angle α between wave vector k and the ray	$\tan\alpha = \frac{Y^2 \sin\theta\cos\theta}{[Y^4 \sin^4\theta + 4Y^2(1-X)^2\cos^2\theta]^{1/2}}$	(8b)
Group velocity (μ) with $Y << 1$	$u^2 = C^2(1-X)$	(9a)	Group velocity with $Y << 1$	$u^2 = c^2(1-X)$	(9b)

TABLE 4

Investigator	Location	Technique	Year	Observational Characteristics	Suggested Source and Comments
			NORTHERN HEMISPHERE		
Liszka and Taylor (1965)	Troms ϕ 69.6°N, 19°E	Faraday rotation of signals	1963	200-300 m. sec.$^{-1}$, travel southward	Auroral zone source. Correlation with magnetic activity.
Goodwin (1968)	Baker Lake 64.3°N, 96°W	Ionosonde	Oct-Nov 1962	Horizontal and vertical wavelengths range 800 ~ 13 km and travel away from winter poles.	No correlation with geomagnetic activity. Associated with D-region absorption.
Klostermeyer (1969)	Lindau 51.7°N, 10°E	Spaced Ionosonde	Winter 1960-1961		Tropospheric Source
Thomas (1959)	Swansea 51.6°N 4°W	Spaced Ionosonde	June 1951-Aug. 1953	40 - 280 m. sec.$^{-1}$travel SE	TID's travelled with no change in characteristics over a distance of 650 km, Velocity increased with geomagnetic activity.
Bramley and Ross (1951) Bramley (1953)	Slough 51.5°N, 0.5° E	Pulsed phase comparison	1948-1952	Daytime observations 35-339 m. sec^{-1} 50-400 km horizontal wavelength	The F-region echo showed quasi-periodic fluctuation of 3-30 min.
Vassuer and Waldteufel (1969)	St. Santin-Nancy 48.7°N, 6°E	Thompson Scatter	Sept. 1967	Vertical wavelength 520 km, horizontal wavelength 4000 km	Auroral zone source. Correlates with magnetic activity.

TABLE 4 (continued)

Investigator	Location	Technique	Year	Observational Characteristics	Suggested Source and Comments
Castle and Faynot (1964)	Garchy 47.3°N 3.5°E	Top and bottom ionosondes	April 1963	100-200 m. sec.$^{-1}$ Irregularities move from higher to lower latitudes under S_q currents	Source located in high latitudes
Elkins and Slack (1969)	Boston 42.5°N 123°E	Transmissions from geo-stationary satellites	1967	50-120 m. sec.$^{-1}$ travel toward equator, horizontal wavelengths 50-100 km	Injection of energetic electrons into auroral zone ionosphere.
Davies and Jones (1971)	Boulder 40°N, 105°W	CW doppler sounder array	1967-1968	145 m. sec.$^{-1}$ velocity vector directed away from winter poles	Sources located in polar regions.
Hunsucker and Tveten (1967)	Boulder 40°N, 105°W	H. F. Back-scatter radar	Winter 1963-1964	80-325 m. sec.$^{-1}$ travel away from poles	52% of the events preceeded by auroral activity.
Davis and da Rosa (1969)	Palo Alto 37.3° N, 122°W	Faraday rotation from satellites	Feb. 1967 Nov. 1968	440-600 m. sec.$^{-1}$ travelling N-S direction horizontal wavelengths 1500 km	Source auroral oval during polar substorms.
Chan and Villard (1962, 1964)	Palo Alto 37.3°N, 122°W	CW doppler sounders	1960-61	400-765 m. sec.$^{-1}$ 30-50 min. periods horizontal wavelengths 1300-1800 km	TID's occurred following sudden commencement of geomagnetic storms.
Georges (1968)	Little Rock 34.5°N, 92°W	CW doppler sounder array	Aug. 1966 Feb. 1967	Medium scale < 300 m. sec.$^{-1}$, large scale > 300 m. sec.$^{-1}$	Large scale irregularities origin near poles

TABLE 4 (continued)

Investigator	Location	Technique	Year	Observational Characteristics	Suggested Source and Comments
Thome (1968)	Puerto Rico 18.3°N, 60°W	Thompson scatter	Summer 1964	200-300 m. sec.$^{-1}$ travel away from poles	Auroral zone source
Reddi and Rao (1971)	Waltair 17.5°N, 83°E	Pulse phase-path sounder	1966-1968	40-230 m. sec.$^{-1}$ periods range 3 - 40 min.	Group speeds are twice the the phase speed.
			SOUTHERN HEMISPHERE		
King (1966)	Hallett 70.3°S. 170.3°E	Ionosonde	Summer 1968	200 m. sec.$^{-1}$ travel away from pole	Infrasonic waves and auroral zone source
Titheridge (1968)	Invercargill 46.3°S, 168.5°E	Faraday rotation from satellites	June-Nov. 1962	50 m. sec.$^{-1}$ Winter periods 15-45 min., Summer periods 15-70 min.	Travelled away from south pole. Source located in polar region.
Wright (1961)	Christchurch 43.5°S, 172.5°E	Ionosonde	1957-1960	406 - 690 m. sec.$^{-1}$ only NS component of the velocity was measured.	TID's observed to a horizontal distance of 1100 km. Positive correlation with magnetic activity.
Munro (1958)	Sydney 34°S, 151.2°E	Three fixed frequency pulsed transmitters	April 1948-March 1957	120 - 150 m. sec.$^{-1}$ Travel away from winter poles	No correlation with magnetic activity
Heisler (1963)	Sydney 34°S, 151.2°E	Spaced Ionosondes	1952-1954	97 - 207 m. sec.$^{-1}$ travel away from winter poles,	TID's travelled with no change in characteristics over a distance of 3000 km. No variation of speed with height.

TABLE 4 (continued)

Investigator	Location	Technique	Year	Observational Characteristics	Suggested Source and Comments
Baker and Gledhill (1965)	Grahms Town 33.3°S 26.5°E	Ionosonde	August 1960	116 m. sec.$^{-1}$ westward direction	Source may be in sunrise conditions of F-Region.
Price (1953, 1955)	Perth 32°S, 116°E	Fixed frequency pulsed transmitters	1949-1952	90 - 330 m. sec.$^{-1}$ winter direction 0° - 6° Eq. N. Summer direction 90° - 180° Eq. N.	No correlation with auroral activity of K-index
Bowman (1965, 1968)	Brisbane 27.5°S, 135.5°E	Ionosonde	Winter 1958	360 m. sec.$^{-1}$ horizontal wavelength 25 - 350 km. Periods 5 - 60 min.	Sources are conjugate high latitude locations, radio and optical auroras and magnetic activity.

TABLE 5

GEOGRAPHIC LOCATION OF THE CW DOPPLER SOUNDER ARRAY

Station	Latitude	Longitude
NASA-MSFC Alabama	34° 39' N.	86° 40' W.
Ft. McClellan, Alabama	33° 44' N.	85° 48' W.
TVA Muscle Shoals, Alabama	34° 46' N.	85° 38' W.
TVA Nciкajack Dam, Tennessee	35° 01' N.	87° 38' W.

APPENDIX

The NASA-MSFC CW doppler sounder array consists of nine CW high frequency field transmitters covering a surface area of about 150 km^2 with radio receivers located in the NASA-MSFC, Huntsville, Alabama. The received signals from all nine transmitters are mixed with stable oscillators of the same nominal frequencies, but are offset several Hz lower. The beat frequencies are then recorded on a slowly moving (one inch per minute) magnetic tape. For data analysis, the tapes are played back at higher speeds into an audio spectrum analyzer. The higher play back speed (for example 15 inches per second) increases all frequencies on the tape by a factor of 900, into the range of about 1 to 5 kHz. The output of the spectrum analyzer is connected to a facsimile recorder, which gives a strip chart record of the Doppler shifted frequency components vs. time.

A block diagram of the equipment for one transmitting station is shown in Figure 14. Three ovenized crystal oscillators are built into one chassis, as shown in the block diagram of Figure 15. Since each of the three transmitters use the same nominal frequencies, the actual frequencies must be slightly different so that they can be distinguished from each other at the receiver. An adjustment on each oscillator module allows the frequency to be offset by about $\pm$ 2 parts per 10^6. The actual frequencies have been set as follows:

Nominal Frequency	Actual Frequencies		
	Unit 1 Muscle Shoals Alabama	Unit 2 Nikajack Dam Tennessee	Unit 3 Ft. McClellan Alabama
4.0125 MHz	4.0125 MHz + 2Hz	4.0125 MHz + 3Hz	4.0125 MHz + 4Hz
4.759 MHz	4.759 MHz + 2Hz	4.759 MHz + 3Hz	4.759 MHz + 4Hz
5.734 MHz	5.734 MHz + 2Hz	5.734 MHz + 3Hz	5.734 MHz + 4 Hz

At the receiving station, the oscillators have been set exactly at the nominal frequencies, so that in the absence of Doppler variations, the offsets of the transmitter oscillators are equal to the beat frequencies. The stability of the oscillators is specified at $\pm$ 1 part per 10^9 per day and $\pm$ 1 part per 10^8 over the ambient temperature range of 0 to 55° C. These variations will not be noticeable, but over a period of a year, the oscillators could drift by as much as 1 Hz. Probably, all the oscillators at both the transmitting and receiving stations will drift in the same direction and the effects will tend to cancel.

The transmitters are modified versions of the Heathkit DK 60B. The transmitting antennas are halfwave dipoles. In order to maximize vertical radiation and minimize horizontal radiation, the height of the dipoles above ground should be between one eighth to one fourth wavelength. Since all three antennas at a site are in one array, a height of approximately 30 feet

has proven to be practical. To null the horizontal radiation in the direction of the receiver, the transmitting antennas at the sites are oriented so that the array is broadside to the receiving site and the ends of the antennas point to the receiver site (NASA-MSFC). Ground waves are not expected to be a problem since the sites are farther than 40 km from the receivers. If a ground wave is received, it can be identified by its stable beat frequency on the doppler records.

A block diagram of the receiving and recording system is shown in Figure 16. The reflected ionospheric echoes from all the nine field transmitters are received by three Hammarlund SP-600-JX-17 communication receivers at three different nominal frequencies. These receivers use single conversion for channel frequencies below 7.4 MHz, and double conversion above 7.4 MHz. In either case, the internal crystal HF oscillator is used instead of the variable frequency oscillator. It is not necessary that the HF oscillator in the signal receiver has the stability of the reference receiver to be mixed with the signal from the reference oscillator. Thus any variations in frequency disappear when the signal intermediate frequency (IF) is mixed with the reference IF.

In order to obtain the accurate timing of ionospheric disturbances, a time code is recorded on channel 4 of the data tape. When the tape is played back for spectrum analysis, the channel 4 output is mixed with whichever data channel is being played back, so that data and timing appear simultaneously on the records.

The output of the timing signal generator is a sine wave during the

first 20 seconds of each minute, and nothing during the last 40. This signal produces a dashed line on spectrograph records, with the leading edge of the dash making the beginning of the minute. The minutes are set into groups of five by a variation in frequency of the output signal. The frequency is 1.0 Hz for five minutes, then 7/8 Hz for 5 minutes, then 1 Hz for five minutes, and so on. This way the minutes can easily be counted from some reference time. To mark the beginning of each hour, a group of five minute marks which would ordinarily be 7/8 Hz is lowered to 3/4 Hz. Thus,the frequency is 3/4 Hz for the first five minutes, 1.0 Hz for the second five, 7/8 Hz for the third five, ..., 1.0 for the last five. For identifying the hour, the frequency of the signal during the first five minutes of the 12th hour (GMT) of the day is lowered to 1/2 Hz instead of 3/4 Hz. The algorithm for selecting the frequency is as follows:

1.0 Hz	when minutes digit = 5, 6, 7, 8, or 9
7/8 Hz	when minutes digit = 0, 1, 2, 3, or 4 and tens minutes digit $\pm$ 0.
3/4 Hz	when minutes digit = 0, 1, 2, 3, or 4 and tens minutes digit = 0 and hours digit $\pm$ 12.
1/2 Hz	when minutes digit = 0, 1, 2, 3, or 4 and ten minutes digit = 0 and hours digit = 12.

The tape recorders used to record data are designed for recording

at one inch per minute only, and will not play back or rewind. The capstar twins at 2 RPM and is machined to a diameter of $1/2\pi$ (0.1596 in). Channels 1, 2, and 3 are used for data, with a timing signal recorded on channel 4. The data tapes are played back on a four channel tape recorder at a speed of 15 inches per second. Each data tape is played back three times; with each playback,one data channel is mixed with the timing channel. The channels are recorded as follows:

Channel 1: 4.0125 MHz, low frequency

Channel 2: 4.759 MHz, middle frequency

Channel 3: 5.734 MHz, high frequency

Channel 4: Timing signal

The output from the tape recorder is spectrum analyzed using a Federal Scientific UA-6B, Ubiguitous audio spectrum analyzer. The output from the spectrum analyzer is fed to a Gifft GPR facsimile recorder, which gives a record of frequency vs. time. The receiving and recording systems are shown in Figure 17 .